Journal of Mammalian Evolution (2022) 29:369–394
https://doi.org/10.1007/s10914-021-09583-4

ORIGINAL PAPER

Comparative Endocranial Anatomy, Encephalization, and Phylogeny of Notoungulata (Placentalia, Mammalia)

Fernando A. Perini[1,2] · Thomas E. Macrini[2,3] · John J. Flynn[2,4] · Kanvaly Bamba[2,5] · Xijun Ni[2,6] · Darin A. Croft[5] · André R. Wyss[7]

Accepted: 25 October 2021 / Published online: 23 November 2021

Abstract

Cranial endocasts are one of the most direct tools available to obtain information about the endocranial cavity of fossil mammals, but few anatomical comparisons have analyzed endocranial data within a phylogenetic framework. Our study combines analyses of new digital endocasts from high-resolution X-ray micro-computed tomography (μCT) for two notoungulates, *Cochilius* sp. and *Notostylops murinus*, with data from published anatomical descriptions and endocasts (prior μCT digital endocasts and natural and extracted plaster endocasts), resulting in 22 endocranial characters (11 new) scored on 20 notoungulates and five outgroups. These data permitted a comparative study of cranial endocasts of notoungulates, an enigmatic group of extinct South American mammals, shedding light on several important issues concerning their phylogenetic relationships. The new endocranial data were integrated into a craniodental and postcranial matrix, resulting in 259 characters across 65 taxa, the most comprehensive character and taxon sampling to date and the only one including a substantial suite of endocranial characters. We further performed ancestral state reconstructions for endocranial characters using parsimony optimization on the resulting phylogenetic trees. Body mass estimates and endocranial volumes were used to calculate Encephalization Quotients (EQs) and Phylogenetic Encephalization Quotients (PEQs), which then were optimized onto the phylogenies. Endocast data from ancestral character state reconstructions bear on relationships among meridiungulates, revealing that many endocast characters may be synapomorphies for Notoungulata and other clades within the group. Notoungulates, in general, display relatively low EQs when compared with Holarctic herbivorous mammals, potentially due to their long history of evolution in isolation in South America during the Cenozoic.

Keywords Endocranial anatomy · CT imaging · Encephalization Quotient (EQ) · Phylogenetic Encephalization Quotient (PEQ) · Meridiungulata · Notoungulata · Phylogeny

✉ Fernando A. Perini
faperini@ufmg.br

[1] Laboratório de Evolução de Mamíferos, Departamento de Zoologia, Instituto de Ciência Biológicas, UFMG, Belo Horizonte 31270-901, Brazil

[2] Department of Vertebrate Paleontology, Division of Paleontology, American Museum of Natural History, Central Park West at 79th Street, New York, NY 10024, USA

[3] Department of Biological Sciences, One Camino Santa Maria, St. Mary's University, San Antonio, TX 78228, USA

[4] Richard Gilder Graduate School, American Museum of Natural History, Central Park West at 79th Street, New York, NY 10024, USA

[5] Department of Anatomy, Case Western Reserve University School of Medicine, 10900 Euclid Ave, Cleveland, OH 44106-4930, USA

[6] Key Laboratory of Vertebrate Evolution and Human Origin, Institute of Vertebrate Paleontology and Paleoanthropology, Xi Zhi Men Wai Street 142, Beijing 100044, China

[7] Department of Earth Science, University of California, Santa Barbara, Santa Barbara, CA 93106, USA

Introduction

"The brain is the most important single mammalian organ, and knowledge of any extinct group must be considered very inadequate until it includes some data on the endocranial anatomy." (Simpson 1933a:1).

As the quotation above from George Gaylord Simpson suggests, knowledge of the soft tissue anatomy of the central nervous system (CNS) is essential for a complete picture of the anatomy and sensory capabilities of extinct mammals, which in fossil mammals can be provided by cranial endocasts, or three-dimensional representations of the space within the endocranial cavity. Indeed, cranial endocasts reveal substantial information about the external anatomy of the brains of mammals and are useful for estimating brain volume (e.g., Jerison 1973; Radinsky 1977, 1978; Kielan-Jaworowska 1983, 1984, 1986; Rowe et al. 2011). Furthermore, cranial endocasts provide data on internal cranial anatomy that are useful for uncovering phylogenetic relationships among fossil and extant taxa (e.g., Kielan-Jaworowska 1997; Macrini et al. 2007b).

Notoungulata, an enigmatic group of extinct South American placental mammals (Simpson 1948, 1980; Patterson and Pascual 1968; Rose 2006; Croft et al. 2020), has been the subject of a number of endocranial studies based on artificial (plaster) and natural cranial endocasts (Simpson 1932, 1933a, b; Patterson 1937; Stirton 1953; Dechaseaux 1958, 1962; Radinsky 1981; Dozo 1997), and more recently of digital endocasts (Macrini et al. 2010, 2013; Dozo and Martínez 2016; Martínez et al. 2019). Many of these works provided descriptive anatomical and volumetric data on notoungulate endocasts that allowed for subsequent comparative studies on relative brain size (e.g., Jerison 1973; Radinsky 1981). Both Jerison (1973) and Radinsky (1981) determined endocranial volumes for endocasts described by previous workers to calculate body mass corrected Encephalization Quotients (EQs) and examine relative brain sizes in notoungulates. Radinsky (1981), like many previous workers (e.g., Simpson 1932, 1933a, b; Patterson 1937; Dechaseaux 1958, 1962), also compared anatomical differences between notoungulate cranial endocasts to study brain evolution in the group. However, none of those anatomical comparisons analyzed data using a phylogenetic framework, nor did they attempt to organize anatomical differences between different notoungulate taxa into characters for phylogenetic analyses.

Our study combines data from previously published anatomical descriptions, natural endocasts, and previously extracted plaster endocasts, with new data from high-resolution X-ray micro-computed tomography (μCT), to undertake the first broad comparative study of cranial endocasts of notoungulates, shedding much needed light on some aspects of the phylogenetic interrelationships of the group as well as the placement of Notoungulata within Placentalia. While molecular evidence supports a relationship with Perissodactyla and other "euungulates" (Buckley 2015; Welker et al. 2015; Westbury et al. 2017) or to Paenungulata within Afrotheria in a combined molecular and morphological analysis (O'Leary et al. 2013), phylogenetic analyses of the relationship of notoungulates to other placental mammals based solely on morphological data have yielded conflicting and generally unresolved results (Cifelli 1993; Horovitz 2004; Billet 2010; Agnolin and Chimento 2011; Billet and Martin 2011). Likewise, analyses of the interrelationships of taxa within the group have not provided a generally well-supported phylogenetic tree, with many relationships still poorly resolved (e.g., Cifelli 1993; Madden 1997; Shockey 1997; Cerdeño and Bond 1998; Nasif et al. 2000; Croft et al. 2004; Flynn et al. 2005; Croft and Anaya 2006; Hitz et al. 2006; Billet et al. 2009; Billet 2010, 2011; Shockey et al. 2012). Morphological phylogenetic analyses have relied primarily on dental, external cranial, and some postcranial characters, and none of these analyses has sampled extensively from the interior of skulls, but this also is the case for morphological phylogenies of most mammalian groups.

We generate a new phylogenetic character matrix of internal cranial anatomy features based on our current study and prior analyses by others (e.g., Gabbert 1997; Macrini et al. 2010, 2013), to more completely sample notoungulate anatomy and hopefully help resolve some of the longstanding phylogenetic uncertainties for the group. The specific aims of our study are as follows: 1) describe new cranial endocast material of notoungulates based on high resolution X-ray μCT imagery of skulls; 2) synthesize new endocast data with published data on notoungulate endocranial cavities from plaster and natural endocasts; 3) score the first extensive matrix of characters based on notoungulate endocranial cavities, and combine these data with a more extensive character matrix sampling from the entire skeleton and dentition, to conduct the most comprehensive phylogenetic analysis to date of notoungulate interrelationships; and 4) to examine relative brain size evolution in notoungulates.

Institutional abbreviations- **AMNH**, American Museum of Natural History, Vertebrate Paleontology Fossil Mammal Collections, New York, NY, USA; **FMNH**, Field Museum of Natural History, Chicago, IL, USA; **MNBA**, Museo Nacional de Historia Natural, Buenos Aires, Argentina; **SGOPV**, vertebrate paleontology collections, Museo Nacional de Historia Natural, Santiago, Chile; **UCMP**, University of California Museum of Paleontology, Berkeley, CA, USA.

Materials and Methods

Specimens

One natural and ten plaster brain endocasts of notoungulates were analyzed from collections at the AMNH and FMNH. In addition, two new digital endocasts were extracted from high resolution X-ray μCT imaging of notoungulate skulls. Anatomical descriptions of the new digital endocasts are provided below.

The litoptern *Tetramerorhinus lucarius* (formerly *Proterotherium cavum*; Simpson 1933b) and the astrapotheres *Trigonostylops wortmani* and *Astrapotherium magnum* were scored based on plaster endocasts and used as outgroups in the analyses. The "condylarths" *Hyopsodus lepidus* and *Phenacodus primaevus* also were used as outgroups and scored based on the descriptions of their endocasts by Orliac et al. (2012) and Simpson (1933a), respectively. A complete list of the specimens examined is provided in Table 1.

Table 1 Cranial endocasts examined in this study (*) and endocranial character data sources

Taxon	Order	Family	Specimen ID	Endocast type	Reference(s)
Adinotherium ovinum	Notoungulata	Toxodontidae	AMNH 55969; FMNH P13107*	Plaster	Patterson (1937); Radinsky (1981)
Astrapotherium magnum	Astrapotheria	Astrapotheriidae	AMNH 55968*	Plaster	Radinsky (1981)
Cochilius sp.	Notoungulata	Interatheriidae	SGOPV 3774*	Digital	this study
Hegetotherium mirabile	Notoungulata	Hegetotheriidae	AMNH 9223*	Plaster	Simpson (1933b)
Homalodotherium cunninghami	Notoungulata	Homalodotheriidae	FMNH P13092*	Plaster	Patterson (1937)
Hyopsodus lepidus	'Condylarthra'	Hyopsodontidae	N/A	N/A	Radinsky (1981)
Interatherium robustum	Notoungulata	Interatheriidae	N/A	N/A	Orliac et al. (2012)
Leontinia gaudryi	Notoungulata	Leontiniidae	N/A	N/A	Radinsky (1981)
Mesotherium sp.	Notoungulata	Mesotheriidae	N/A	N/A	Dechaseaux (1962)
Miocochilius anomopodus	Notoungulata	Interatheriidae	N/A	N/A	Stirton (1953); Radinsky (1981)
Nesodon imbricatus	Notoungulata	Toxodontidae	AMNH 55971*; FMNH P13076	Plaster	Patterson (1937); Radinsky (1981)
Notostylops murinus	Notoungulata	Notostylopidae	FMNH P13319*	Digital	Simpson (1932, 1933a); this study
Notostylops pendens	Notoungulata	Notostylopidae	AMNH 28614*	Plaster	Simpson (1933a)
Oldfieldthomasia debilitata	Notoungulata	Oldfieldthomasiidae	AMNH 28780*	Natural	Simpson (1932)
Pachyrukhos typicus	Notoungulata	Hegetotheriidae	AMNH 9525; AMNH 15918	N/A	Dechaseaux (1962); Radinsky (1981)
Paedotherium insigne	Notoungulata	Hegetotheriidae	AMNH 45914	N/A	Radinsky (1981); Dozo (1997)
Phenacodus primaevus	'Condylarthra'	Phenacodontidae	N/A	N/A	Simpson (1933a)
Proadinotherium muensteri	Notoungulata	Toxodontidae	AMNH 55970*	Plaster	Patterson (1937); Radinsky (1981)
Protypotherium australe	Notoungulata	Interatheriidae	N/A	N/A	Radinsky (1981)
Protypotherium sp.	Notoungulata	Interatheriidae	AMNH 9246*	Plaster	Simpson (1933b); Radinsky (1981)
Pseudotypotherium pseudopachygnathum	Notoungulata	Mesotheriidae	N/A	N/A	Radinsky (1981)
Rhynchippus equinus	Notoungulata	Notohippidae	FMNH P13420*	Plaster	Patterson (1937); Radinsky (1981)
Rhyphodon sp.	Notoungulata	Isotemnidae	AMNH 29414*	Plaster	Simpson (1933a)
Tetramerorhinus lucarius	Litopterna	Proterotheriidae	AMNH 9245*	Plaster	Simpson (1933b)
Toxodon platensis	Notoungulata	Toxodontidae	N/A	N/A	Dechaseaux (1962)
Trachytherus spegazzinianus	Notoungulata	Mesotheriidae	N/A	N/A	Patterson (1934)
Trigonostylops wortmani	Astrapotheria	Trigonostylopidae	AMNH 28700	Plaster	N/A
Typotheriopsis internum	Notoungulata	Mesotheriidae	FMNH P14420*	Plaster	Patterson (1937)

A skull of *Notostylops murinus* (FMNH P13319) from the Gran Barranca, Argentina (Simpson 1948), from a fauna corresponding to the Casamayoran SALMA (Cifelli 1985), was imaged using high-resolution x-ray CT, and a digital endocast was extracted (see below). This skull represents an advanced growth-stage juvenile individual with milk teeth still in place (dP2-4, M1-2; Riggs and Patterson 1935; Simpson 1948). We used this endocast to score brain endocast phylogenetic characters along with an incomplete natural endocast of an adolescent individual of *Notostylops pendens* (AMNH 28614; Simpson 1933a, 1948) and a description of an incomplete endocast of *Notostylops ampullaceus* by Simpson (1932), an apparent adult specimen (Simpson 1948). We note that the endocast characters used in our study vary little with ontogeny, as they do not deal with shape or allometric relationships (see Macrini et al. 2007c). The inner ear of the juvenile specimen of *N. murinus* (FMNH P13319), previously described by Macrini et al. (2010), was used to score inner ear characters for this taxon in our matrix. Ekdale (2010) demonstrated that adult sizes of several inner ear characters, such as the arcs of semicircular canals, are achieved before the inner ear is fully functional in marsupials (*Monodelphis domestica*). As there is overlap between the characters examined by Ekdale (2010) and those used by Macrini et al. (2010), we think that the dimensions for the inner ear of the juvenile specimen of *N. murinus* (FMNH P13319), a placental mammal, should be representative of those of an adult.

CT Scanning and Digital Endocast Extraction

The two skulls analyzed for digital endocast reconstruction were scanned in their entirety in the coronal plane at the Center for Quantitative X-ray Imaging at Penn State University (www.cqi.psu.edu) in University Park, PA using the HD-600 industrial scanner. Scan data were reconstructed as 1024 × 1024 pixel, 16-bit Tiff slices (e.g., images). The scan of the skull of *N. murinus* resulted in 1599 slices, with reconstructed pixel size in the X and Y planes of 0.062 mm and interslice spacing of 0.0684 mm. The scan of the skull of *Cochilius* sp. (SGOPV 3774) resulted in 1066 slices, with reconstructed pixel size in the X and Y planes of 0.060 mm and interslice spacing of 0.0690. Digital endocasts were extracted using the segmentation tools of Avizo 5.0 (2008, Mercury Computer Systems, <www.mc.com>).

Phylogenetic Character Matrix and Analyses

A total of 22 endocranial characters, 11 of them new, were scored based on specimens of 20 notoungulate taxa and five outgroups (Table 1) and data in the literature (Appendices I and II). Measurements relevant to the phylogenetic characters were taken from specimens via digital measurement tools for CT reconstructions, using calipers that are accurate to the nearest 0.05 mm for physical endocasts, or using a ruler and scale bars for figured specimens in the literature. Figure 1 illustrates how these measurements were taken. All measurements were taken three times and then averaged (Table 2). Endocast length was measured by maximum

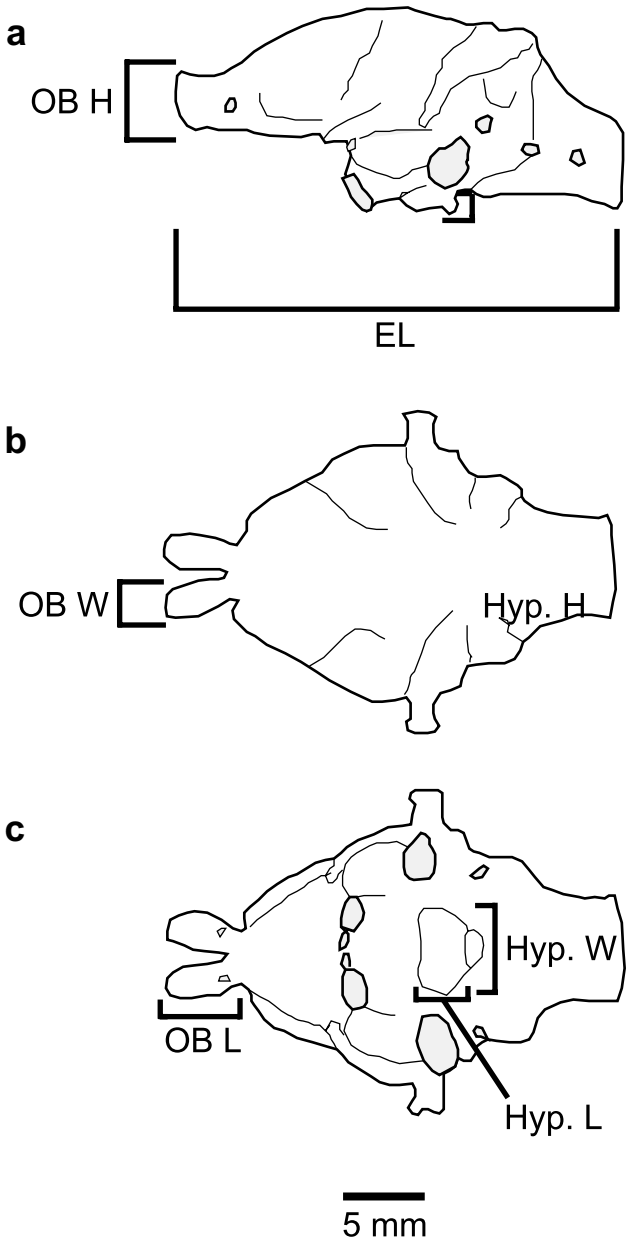

Fig. 1 Line drawings of a natural endocast of *Rhynchippus equinus* (FMNH P13410) in **a**, left lateral; **b**, dorsal; and **c**, ventral views showing how measurements reported in Table 3 were taken. Images redrawn from Fig. 75 of Patterson (1937). Abbreviations: EL, endocast length; H, height; Hyp., hypophysis; L, length; OB, olfactory bulb; W, width

anteroposterior distance from the tip of the olfactory bulbs to the foramen magnum. Right olfactory bulbs were measured unless otherwise noted. For both the olfactory bulbs and the hypophysis, length was measured as maximum anteroposterior distance, and height was measured as the maximum dorsoventral distance. Width was measured on a single olfactory bulb, as the maximum mediolateral distance perpendicular to the midline of the endocast. The width of the hypophysis also was measured perpendicular to the midline of the endocast.

These endocranial data were integrated into a larger character matrix that was assembled from previously published phylogenies (Cifelli 1993; Gabbert 1997; Shockey 1997; Croft et al. 2003; Reguero et al. 2003; Flynn et al. 2005; Croft and Anaya 2006; Hitz et al. 2006; Billet 2010, 2011; Shockey et al. 2012), but also adding scoring for 11 original characters (Online Resources 1 and 2). To create the initial character list, publications were scanned for character descriptions and coding, which were incorporated into the matrix and crosschecked to avoid redundancy. In some cases, the characters were modified or reworded from the original source, as indicated in Online Resource 1. The resulting matrix includes 99 characters from the dentition (three of which are new), 72 from the exterior of the skull, 25 from the inner ear (characters and data from Macrini et al. 2013), and 41 from the postcranium, in addition to the 22 endocranial characters scored for the first time here across all taxa, for a total of 259 characters examined across 65 taxa (57 notoungulates, eight outgroups) (Online Resource 1). Despite some concerns about the codependence of some inner ear characters with allometric traits, which may in turn affect the influences of these characters on phylogenetic trees (Billet et al. 2015a), most studies have shown that, in general, inner ear characters provide phylogenetically significant and diagnostic information regardless of allometry (Billet and Muizon 2013; Macrini et al. 2013; Ravel and Orliac 2014; Orliac and O'Leary 2016). This issue certainly deserves further scrutiny, but some recent studies suggest that the influence of allometry may be weak and play a secondary role to phylogenetic signal (e.g. Billet et al. 2015b). Taxa were scored based on direct examination of specimens deposited in the AMNH and FMNH and previously published descriptions. Character polarity was determined by outgroup analysis. For the outgroups, taxa representing other orders of Meridiungulata (Pyrotheria, Astrapotheria, Xenungulata, and Litopterna) and basal "ungulates" (*Phenacodus primaevus* and *Hyopsodus lepidus*) were selected, as detailed above. The complete matrix is available as Project 667 in Morphobank (http://morphobank.org/permalink/?P667) and in Online Resource 2.

Parsimony analyses were conducted using TNT (Goloboff et al. 2008b), applying new technology algorithms (Goloboff 1999; Nixon 1999) to search for the shortest trees that subsequently were used to perform standard TBR searches. All characters were considered unordered, as there is no definitive a priori justification for ordering any of them. Branch

Table 2 Measurement data from endocasts used in this study. Abbreviations: EL, endocast length; H, height; Hyp., hypophysis; L, length; OB, olfactory bulb; N/A, not applicable; W, width; ?, missing data (e.g., could not be measured because of damage to the specimen). Measurements are presented in mm

Taxon	Specimen #	EL	OB L	OB W	OB H	OB W/H	OB W/L	Hyp. L	Hyp. W	Hyp. W/L	Hyp. H
Adinotherium ovinum	AMNH 55969	100.6	9.16	12.94	8.9	1.45	1.41	21.06	15.7	0.75	?
Astrapotherium magnum	AMNH 55968	217.25	33.05	12.6	26.45	0.48	0.38	?	?	?	?
Cochilius sp.	SGOPV 3774	40.4	7.3	3.7	7.7	0.48	0.51	4.9	4.1	0.84	1.2
Hegetotherium mirabile	AMNH 9223	59.4	10.5	6.7	7.4	0.91	0.64	7.7	6.9	0.90	?
Homalodotherium cunninghami	AMNH 55967	152.5	23.2	11.3	19.3	0.59	0.49	?	?	?	?
Hyopsodus lepidus	AMNH 143783	32.37	7.47	4.51	5.66	0.80	0.60	?	?	?	?
Miocochilius anomopodus	UCMP 39651	?	16.4	6.85	?	N/A	0.42	?	?	?	?
Nesodon imbricatus	AMNH 55971	176.2	17.2	18.3	15.25	1.2	1.06	15.25	15	0.98	?
Notostylops murinus	FMNH P13319	46.5	8.9	5.7	8.5	0.67	0.64	5.1	2.5	0.49	1.3
Notostylops pendens	AMNH 28614	57.2	?	?	?	N/A	N/A	10.7	10	0.93	?
Oldfieldthomasia debilitate	AMNH 28780	51.8	10.8	5.15	5.7	0.90	0.48	?	?	?	?
Phenacodus primaevus	AMNH 4369	10.9	1.9	1.8	1.5	0.95	1.2	?	?	?	?
Proadinotherium muensteri	AMNH 55970	130.3	6.35	7.1	5.25	1.35	1.12	20.8	20.35	0.98	13.8
Protypotherium sp.	AMNH 9246	45.1	4.9	4.56	8.4	0.54	0.93	?	?	?	?
Rhynchippus equinus	AMNH 55963	113.3	23.15	14.2	24.1	0.59	0.61	13.3	19.4	1.46	11.1
Rhyphodon sp.	AMNH 29414	99.2	18.2	11.6	14.3	0.81	0.64	9.8	10.45	1.07	?
Tetramerorhinus lucarius	AMNH 9245	96.8	14.8	5.65	10.8	0.52	0.38	?	?	?	?
Typotheriopsis internum	AMNH 55964	101.56	11.3	8.5	12.5	0.68	0.75	?	?	?	?

support was provided by a bootstrap analysis (Felsenstein 1985) with 1000 replicates and by Bremer support/decay index analysis (Bremer 1994).

The matrix was analyzed further using an implied weighting (IW) algorithm, which weights characters based on their homoplasy (Goloboff 1993). Weighting against homoplasy reportedly improves the robustness of phylogenetic analyses of morphological data by improving stability of clades compared with analyses that weight characters equally (Goloboff et al. 2008a, 2018a, b). The value of the concavity constant (K-value) applied was the default value (K = 3), which down-weights considerably against homoplastic characters. Branch support in this analysis was determined by relative Bremer support (Goloboff and Farris 2001).

Analysis of Evolution of Endocast Characters

Using parsimony ancestral state reconstruction in Mesquite (version 3.61) (Maddison and Maddison 2019), a selected subset of endocranial characters was mapped onto a pruned phylogenetic tree including only the taxa with available endocasts, to examine the evolution of the endocranium (brain) of notoungulates (Fig. 6). The topology of this pruned tree was essentially that of the equally weighted (EW) analysis but with two differences, regarding the relationships between *Tetramerorhinus lucarius*, Astrapotheria (*Trigonostylops wortmani* and *Astrapotherium magnum*), and *Notostylops murinus*, which form a polytomy, as well as *Typotheriopsis internum*, *Pseudotypotherium pseudopachygnathum*, and *Mesotherium cristatum*. In those two cases, we resolved the polytomies with the topology found in the IW analysis, which is fully resolved for these taxa. The ancestral state reconstruction analyses utilized DELTRAN, delayed transformations, for optimization of missing or ambiguously optimized character states (Farris 1970).

Encephalization Quotient Analysis

Encephalization Quotients (EQs) and Phylogenetic Encephalization Quotients (PEQs), body mass estimates, and endocranial volumes for selected notoungulates are presented in Table 3. Volumes of the digital endocasts examined directly in this study were measured using Avizo. Endocranial volumes of other notoungulates were obtained from the literature as reported by the original authors (Table 3). Other authors either directly measured volumes of endocasts using volume displacement in water (Jerison 1973; Radinsky 1981), or for endocasts that could not be measured directly, the endocast volume was estimated by the original author by treating the space as a cylinder (Jerison 1973). Notoungulate body mass estimates were taken from the literature (Table 3; Online Resource 3).

Encephalization Quotients (EQs) were calculated for all taxa using several approaches (Table 3). First, we used the widely applied EQ equations for mammals from Jerison (1973) and Eisenberg (1981). Encephalization values also were calculated by deriving an equation empirically from the Phylogenetic EQ (PEQ) introduced by Ni et al. (2019). This approach calculates an encephalization quotient from phylogenetic generalized least squares (PGLS), an analysis that also corrects for phylogenetic nonindependence between data points (Symonds and Blomberg 2014). The resulting equation for the taxa analyzed in this study can be expressed as PEQ = EXP (lnEV—0.6607 * lnBM + 2.5023), where EV = Endocranial Volume and BM = Body Mass, and this equation was used to calculate PEQ values for each species. These values were mapped using squared-change parsimony for continuous data (Maddison 1991) on a pruned topology of the trees generated from our phylogenetic analysis as described above, but in this case including only the taxa for which was possible to calculate EQ and PEQ values. For this analysis, we used the Jerison (1973) EQ equation, which allowed for direct comparison with other studies using the same equation (e.g., Boddy et al. 2012), in addition to our new empirically determined PEQ values that incorporate the phylogenetic context for comparative encephalization in the Notoungulata clade.

Results

Description of New Digital Endocasts of Notoungulata

***Cochilius* sp.** (SGOPV 3774; Fig. 2) — This endocast description of *Cochilius* sp., from the Upeo Fauna of the Abanico Formation of Chile (likely Deseadan SALMA [late Oligocene] in age; see age discussion and analyses of the inner ear in Macrini et al. 2013), represents the first for this taxon. In lateral view (Fig. 2a, a'), the degree of cranial flexure (sensu Macrini et al. 2007a) is 20˚, and the olfactory bulb casts are dorsoventrally deep. The endocast is widest across the posterior portions of the cerebral hemisphere casts. Linear measurements and aspect ratios for this endocast are presented in Table 2. The endocranial volume of this endocast was measured as 6,839 mm^3, and the olfactory bulb volume (the total from both left and right bulbs) is 292 mm^3. Based on these numbers, the olfactory bulbs comprise 4.3% of the total endocast volume.

Forebrain— The cast of the cerebrum is moderately gyrencephalic; it displays (from medial to lateral) a lateral sulcus, Sylvian sulcus, an anterior rhinal fissure, and a rhinal fissure (Fig. 2). In dorsal view, a pronounced circular fissure separates each olfactory bulb from the isocortex of the cerebrum. The annular ridge of the frontal is the

Table 3 Encephalization Quotient (EQ) and Phylogenetic Encephalization Quotient (PEQ) calculations for notoungulates and outgroups, using different methods to assess encephalization. Abbreviations: EQ (Eisenberg), calculated using equation from Eisenberg (1981): EQ = EV / (0.055 * [BM]$^{0.74}$); EQ (Jerison), calculated using equation from Jerison (1973): EQ = EV / (0.12 * [BM]$^{0.67}$); PEQ, Phylogenetic Encephalization Quotient: PEQ = EXP (lnEV-0.6835 * lnBM + 3.0113); EV, endocranial volume; BM, body mass

Species	EV (mL)	EV source	Mass estimate (g)	Mass source	EQ (Eisenberg)	EQ (Jerison)	PEQ (this study)
Adinotherium ovinum[a]	90	Jerison (1973)	88,000	Jerison (1973)	0.36	0.36	0.76
Adinotherium ovinum[b]	110	Radinsky (1981)	88,000	Jerison (1973)	0.44	0.47	0.93
Astrapotherium magnum	425	Radinsky (1981)	800,000–1,200,000	Croft et al. (2020)	0.24—0.33	0.30—0.39	0.60—0.80
Cochilius sp.	6.8	this study	2,050	Scarano et al. (2011)	0.48	0.34	0.75
Hegetotherium mirabile	20	Radinsky (1981)	5,100	Jerison (1973)	0.66	0.57	1.23
Homalodotherium cunninghami	223	Radinsky (1981)	300,547	Croft (2000)	0.36	0.40	0.82
Hyopsodus lepidus	2.8	Orliac et al. (2012)	326—854	Orliac et al. (2012)	0.34—0.70	0.25—0.48	0.56—1.09
Interatherium robustum	8	Radinsky (1981)	1,400	Radinsky (1981)	0.68	0.52	1.15
Leontinia gaudryi	380	Radinsky (1981)	126,000—173,000	Radinsky (1981)	0.92—1.16	0.98—1.21	2.03—2.52
Miocochilius anomopodus	30	Radinsky (1981)	12,000	Croft (2016)	0.52	0.46	0.99
Nesodon imbricatus	230	Radinsky (1981)	293,661	Croft (2000)	0.38	0.42	0.86
Notostylops murinus[c]	17	Jerison (1973)	5,300–7,700	Radinsky (1981)	0.41—0.54	0.35—0.45	0.76—0.98
Notostylops murinus[d]	9.8	this study	5,300–7,700	Radinsky (1981)	0.24—0.31	0.20—0.26	0.44—0.57
Notostylops pendens	9.7	Jerison (1973)	5,300–7,700	Radinsky (1981)	0.24—0.31	0.20—0.26	0.43—0.56
Proadinotherium muensteri	145	Radinsky (1981)	40,300	Radinsky (1981)	1.03	0.99	2.10
Protypotherium australe	17	Radinsky (1981)	5,860	Scarano et al. (2011)	0.50	0.42	0.92
Protypotherium sp.	12	Jerison (1973)	5,278	Scarano et al. (2011)	0.38	0.32	0.70
Pseudotypotherium pseudopachygnathum	60	Radinsky (1981)	22,000—30,000	Radinsky (1981)	0.53—0.67	0.50—0.62	1.06—1.31
Rhynchippus equinus	112	Radinsky (1981)	32,000	Radinsky (1981)	0.94	0.89	1.90
Rhyphodon sp.	45	Radinsky (1981)	28,000—38,000	Radinsky (1981)	0.33—0.42	0.32—0.39	0.68—0.83
Tetramerorhinus lucarius	60	Radinsky (1981)	18,000	Radinsky (1981)	0.77	0.70	1.50
Toxodon sp.	570	Jerison (1973)	1,000,000–1,200,000	Croft (2016)	0.33—0.38	0.40—0.45	0.81—0.92
Typotheriopsis internum	85	Radinsky (1981)	24,000—33,000	Radinsky (1981)	0.70—0.89	0.67—0.82	1.41—1.75

[a]FMNH P13110

[b]FMNH P13108

[c]MNBA 10506

[d]FMNH P13319

bony feature responsible for forming the circular fissure on an endocast (Macrini et al. 2007a, b). The rhinal fissure, marking the ventral edge of the isocortex and its boundary with the piriform cortex, is discontinuous, with separate anterior and posterior portions. A thin sliver of the piriform cortex is visible in dorsal view, but the cortex is more prominent in lateral and ventral views (Fig. 2). The lateral cerebral venous sinus is visible on the right side of the endocast, running adjacent to the posterior portion of the rhinal fissure; this sinus is not visible on the left side of the endocast (Fig. 2b, b'). The median sulcus, which separates the right and left cerebral hemispheres, is only visible on the anterodorsal portion of the cerebral hemisphere as a shallow, undulating sulcus (Fig. 2b, b').

Midbrain— The midbrain is not exposed on this endocast, as it is covered dorsally by the isocortex and obscured ventrally by the piriform cortex and hindbrain.

Hindbrain— The small, rounded cerebellar hemispheres and the vermis are clearly visible in the dorsal view of the hindbrain (Fig. 2b, b'). The paired paraflocculi representing the space in the subarcuate fossae, are cone-shaped in *Cochilius* (Fig. 2). (Some authors, such as Lopez-Torres et al. 2020, equate the paraflocculus with the petrosal lobule, but some others, such as Sánchez-Villagra 2002, consider the

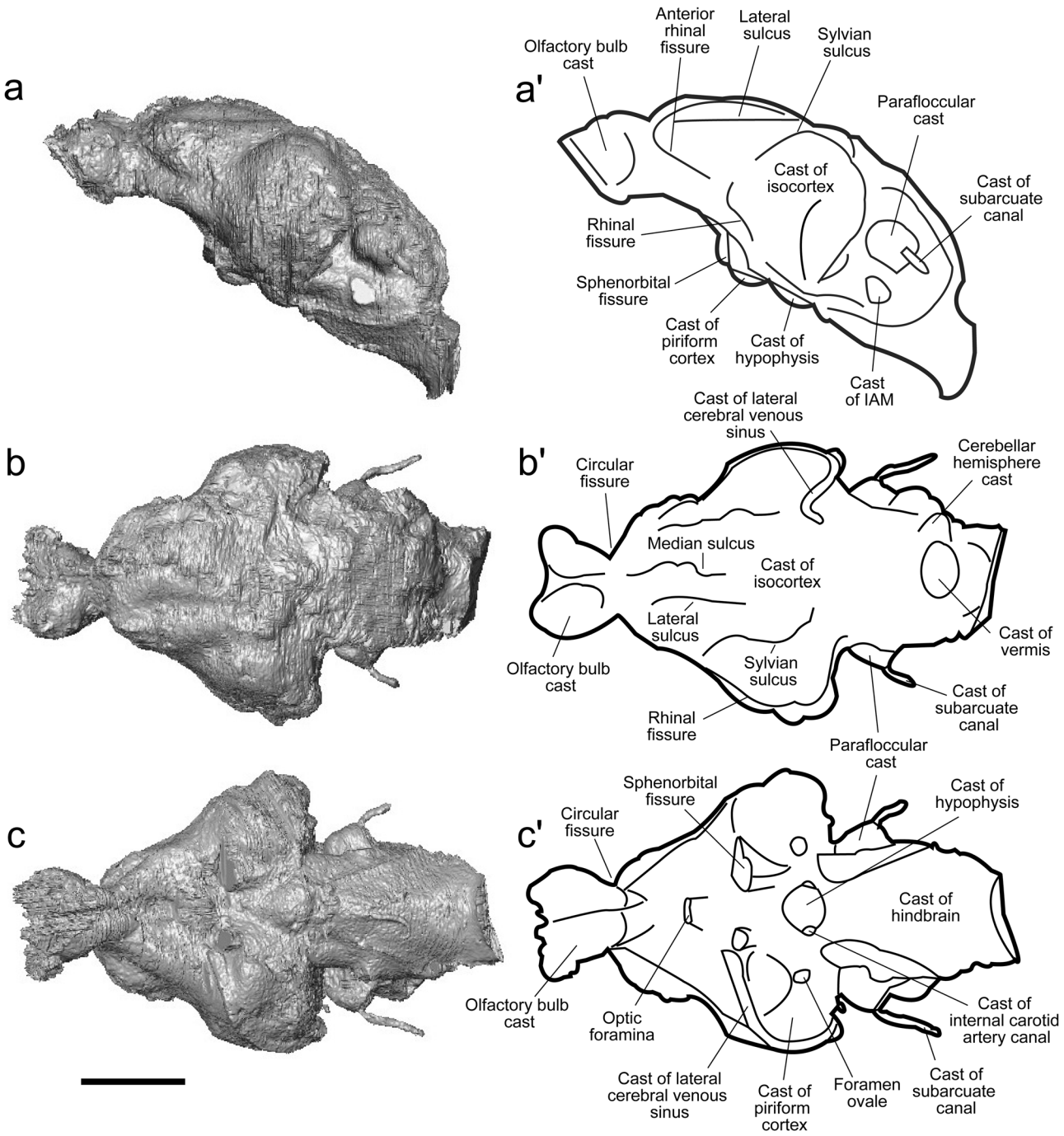

Fig. 2 Digital cranial endocast of *Cochilius* sp. (SGOPV 3774) in **a**, left lateral; **b**, dorsal; and **c**, ventral views. Line drawings of the cranial endocast with anatomical labels in **a'**, left lateral; **b'**, dorsal; and **c'**, ventral views. Abbreviation: IAM, internal acoustic meatus (for cranial nerves VII and VIII). Scale bar equals 1 cm

petrosal lobe to be part of the paraflocculus.) The subarcuate canal (=petromastoid canal) is clearly visible on both sides of the skull (coronal CT slices C906-977), extending from the subarcuate fossa to the mastoid antrum, an air-filled cavity in the petrosal (Gray 1977). In humans, this canal, which is wide in children and narrower in adults, houses the subarcuate artery and vein (Krombach et al. 2002). Few details are visible on the ventral surface of the hindbrain, as the boundaries of the pons and medulla oblongata are not discernible (Fig. 2c, c'). These brain features were likely obscured by

cisterns within the subarachnoid space and other structures within the meningeal space, thus precluding their impressions on the cranial (inner) surface of the basioccipital bone.

Cranial nerves— The endocranial surface of the cribriform plate leaves its impression on the ventral surface of the olfactory bulbs. Fibers of the olfactory nerve (cranial nerve [CN] I) passed through the various openings of the cribriform plate. Paired optic foramina accommodated the optic nerve (CN II); these foramina appear confluent. Cranial nerves III, IV, V_1, V_2, and VI presumably passed through the sphenorbital fissure. The mandibular branch of the trigeminal nerve (CN V_3) likely passed through the foramen ovale, as in other mammals. Cranial nerves VII and VIII undoubtedly passed through the internal acoustic meatus. The jugular foramen for exit of cranial nerves IX, X, XI, and XII is not clearly visible.

Midventral endocast surface— The most prominent feature on this portion of the endocast is the hypophysis, which housed a portion of the pituitary gland. The hypophysis is oval (Fig. 2c, c'), with its long axis oriented in the coronal plane. Portions of the canals for the internal carotid arteries are visible on the posterolateral edges of the hypophysis (Fig. 2c, c').

Notostylops murinus (FMNH P13319; Fig. 3) — This description of the digital endocast of *N. murinus*, from Casamayoran SALMA (middle Eocene) faunas of Argentina, is a supplement to the published descriptions of a natural endocast of another specimen of *N. murinus* (Simpson 1932) and a plaster endocast for its near relative, *N. pendens* (Simpson 1933a). The right side of this skull appears to exhibit a slight obliquely oriented dorsoventral distortion; this shear is evident when comparing the right and left sides of the digital endocast (Fig. 3). Linear measurements and aspect ratios for this endocast are presented in Table 2. The endocranial volume was measured as 9,807 mm^3, and the total olfactory bulb volume (both left and right) is 629 mm^3. The olfactory bulbs, which are much larger compared to overall endocast size than in *Cochilius*, comprise about 6.4% of the total endocast volume in *Notostylops*. The cranial flexure of *Notostylops* is 34°, which is substantially greater than that of *Cochilius*.

Forebrain— The cerebrum is mostly lissencephalic (smooth); however, it does display a suprasylvian sulcus and rhinal fissure, both of which are more obvious on the left than the right side of the endocast (Fig. 3). The median sulcus clearly separates the right and left cerebral hemispheres along the midsagittal plane. The rhinal fissure appears continuous on the left lateral side (Fig. 3a, a'), and is best seen in dorsal view on the right side (Fig. 3b, b'). A small portion of the piriform cortex is visible in dorsal view on both the left and right sides of the endocast and is most evident on the right side (Fig. 3b, b'). A deep circular fissure separates the prominent olfactory bulbs from the cerebral hemispheres.

Midbrain— Similar to the endocast of *Cochilius*, the midbrain is not exposed in *Notostylops*. The midbrain was covered dorsally by the isocortex and obscured ventrally by the piriform cortex and the hindbrain as in many extant mammals (e.g., *Monodelphis domestica*; Macrini et al. 2007c).

Hindbrain— The vermis is clearly visible on the dorsoposterior portion of the cerebellum (Fig. 3a, b), but the cerebellar hemispheres are not distinct from the rest of the cerebellum. The paraflocculi are broad and rounded in *Notostylops*. Similar to the endocast of *Cochilius*, the boundaries of the pons and medulla oblongata are not discernible on the ventral surface of the hindbrain of *Notostylops* (Fig. 3c, c').

Cranial nerves— The endocranial surface of the cribriform plate is not as well preserved in the *Notostylops* skull as in *Cochilius*; therefore, the olfactory nerve fibers (CN I) are not visible (Fig. 3a, c). As in *Cochilius*, the paired optic foramina (for passage of CN II) appear to be confluent. As there is no clear evidence for a foramen rotundum in *Notostylops* (Simpson 1933a), the maxillary branch of the trigeminal nerve (CN V_2) presumably passed through the sphenorbital fissure, along with CNs III, IV, V_1, and VI, as is typically seen in placental mammals. The paired foramina ovale (for CN V_3) are oriented anteroposteriorly (Fig. 3a, c; Simpson 1933a) rather than ventrally as in *Cochilius*. The internal acoustic meatus clearly shows two nerve canal pathways for CNs VII and VIII (Fig. 3a, a'). The jugular foramina for exit of CNs IX, X, and XI, and the hypoglossal foramina for exit of CN XII, are not clearly visible on the digital endocast but are clear on a natural endocast of *Notostylops* (AMNH 28614; Simpson 1933a).

Midventral endocast surface— The hypophysis is oval (Fig. 3c, c'), with its long axis oriented anteroposteriorly. The internal carotid arteries are not visible.

Phylogenetic Analysis

The unweighted parsimony analysis of the complete phylogenetic matrix (259 characters scored for 57 notoungulates and eight outgroups) resulted in 112 most parsimonious trees, each measuring 935 steps in length (CI = 0.311; RI = 0.678) (strict consensus shown in Fig. 4a). The implied weighting (IW) analysis produced two most parsimonious trees, and their strict consensus is shown in Fig. 4b.

In the unweighted tree, *N. murinus* (generally considered to be a notoungulate) forms a polytomy with *Pyrotherium* (Pyrotheria), *Carodnia* (Xenungulata), and a monophyletic clade including the rest of the species traditionally placed within Notoungulata (Fig. 4a). However, the IW analysis recovered *Pyrotherium* and *Carodnia* as sister taxa, and a clearly monophyletic Notoungulata, with *N. murinus* as the first-diverging taxon within this clade (Fig. 4b). Within Notoungulata, our results from both analyses support the monophyly of Toxodontia and Typotheria (sensu Cifelli

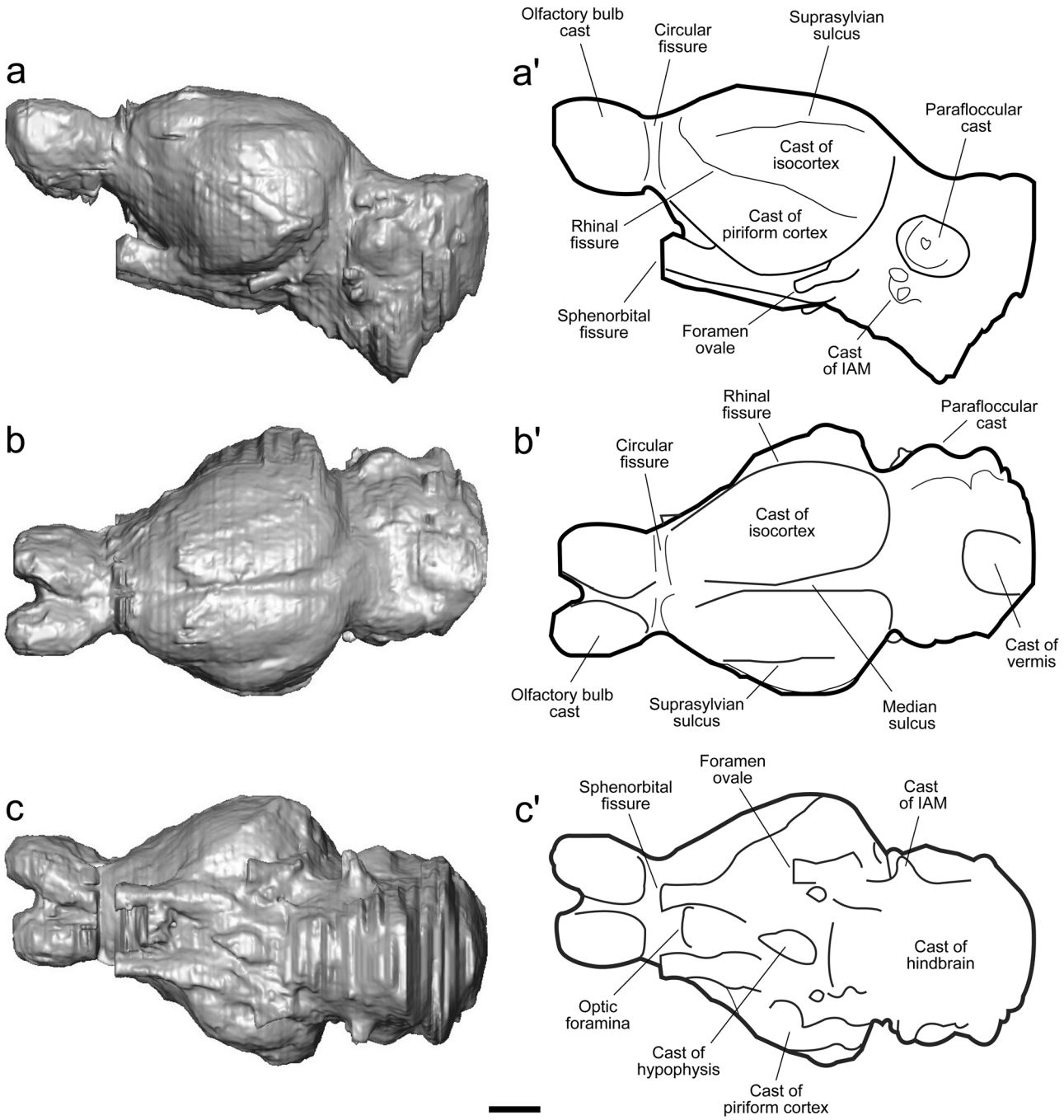

Fig. 3 Digital cranial endocast of *Notostylops murinus* (FMNH P13319) in **a**, left lateral; **b**, dorsal; and **c**, ventral views. Line drawings of the cranial endocast with anatomical labels in **a'**, left lateral; **b'**, dorsal; and **c'**, ventral views. Abbreviation: IAM, internal acoustic meatus (for cranial nerves VII and VIII). Scale bar equals 5 cm

1993). In the unweighted analysis, a clade formed by *Anisotemnus distentus* and *Thomashuxleya externa* (traditionally "isotemnids") forms a polytomy with Toxodontia and Typotheria, although both species are included within Toxodontia in the IW analysis, forming a clade with several other taxa traditionally classified as Isotemnidae or Homalodotheriidae. The best known and sole henricosborniid in the analysis, *Simpsonotus*, forms an early diverging taxon within Notoungulata in both analyses. The only member of Homalodotheriidae in this analysis, the best-known member of the group (*Homalodotherium*), is among the basalmost taxa in the Toxodontia radiation in the unweighted analysis, but instead is nested within an unexpectedly monophyletic Isotemnidae in the IW analysis (e.g., Isotemnidae is termed

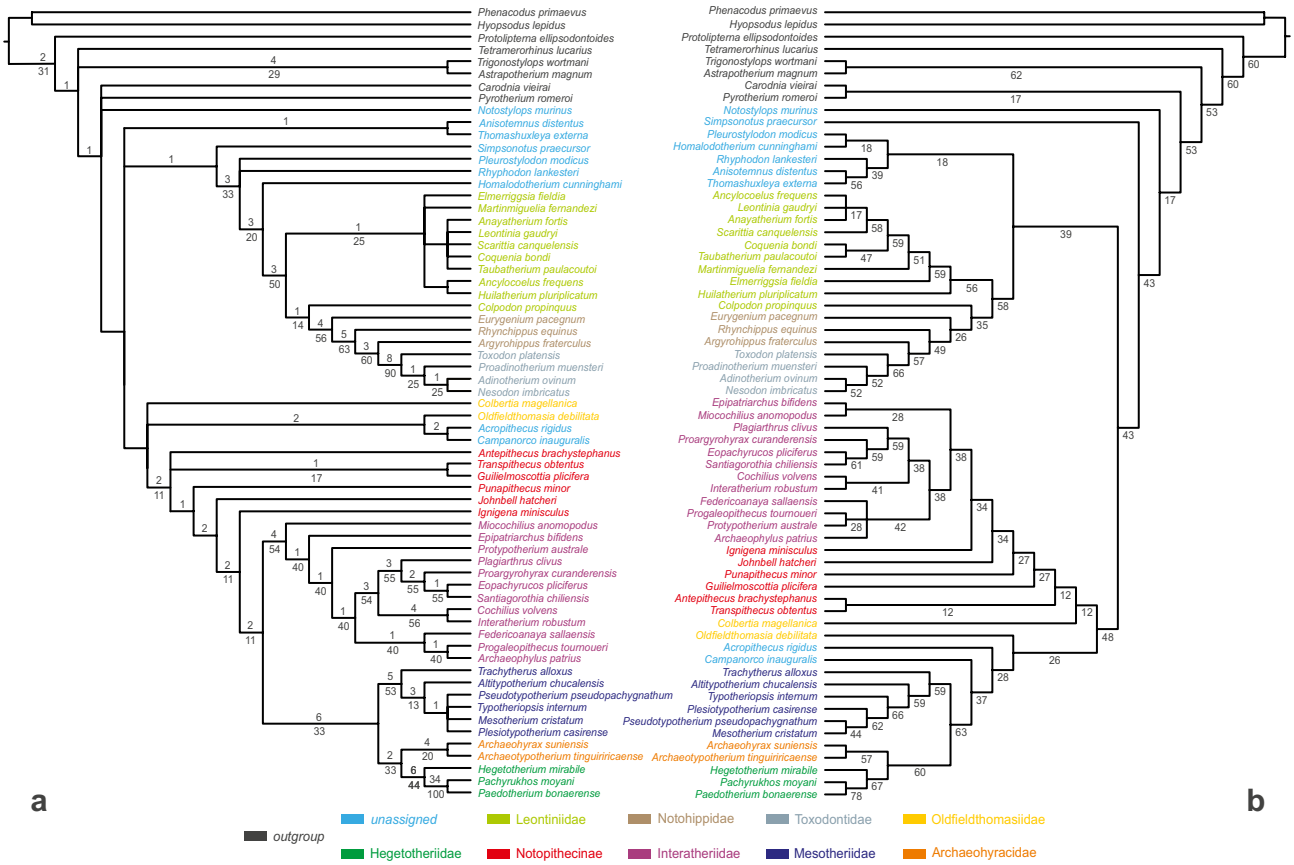

Fig. 4 Strict consensus parsimony trees from analyses of complete phylogenetic matrix of 259 characters examined across 65 taxa (57 notoungulates and eight outgroups): **a,** unweighted; **b**, implied weighting. Numbers above branches in the unweighted tree (**a**) are Bremer support values and below branches are Bootstrap values; numbers below branches in the implied weighting tree (**b**) are relative Bremer support values. Color of taxon names corresponds to their traditional family assignments in the key; light blue are unassigned notoungulates of enigmatic or controversial relationships, and black are outgroups

"demonstrably nonmonophyletic" in Wyss et al. 2018). Species traditionally assigned to Isotemnidae represent a paraphyletic assemblage near the base of either Notoungulata or Toxodontia in the unweighted analysis, consistent with prior notions of paraphyly of this group. But as noted above, Isotemnidae are monophyletic in the IW analysis, albeit with relatively weak support; this clade, inclusive of the homalodotheriid *Homalodotherium*, forms the sister clade to all other toxodontians in the IW analysis. Leontiniidae is monophyletic in both analyses, exclusive of *Colpodon*, although relationships within the clade remain poorly resolved in the unweighted analysis. Both analyses surprisingly exclude *Colpodon propinquus* from the clade formed by other members traditionally assigned to this family, as monophyly of Leontiniidae has had substantial support in prior phylogenetic analyses (e.g., Shockey et al. 2012; see discussion in Wyss et al. 2018). *Colpodon* is instead positioned at the base of a toxodontian clade of Notohippidae plus Toxodontidae in both analyses. As suggested by many previous studies (e.g., Cifelli 1993; Shockey 1997; Billet 2011; Shockey et al. 2012; Wyss et al. 2018), Notohippidae is a paraphyletic assemblage at the base of a monophyletic Toxodontidae or potentially a clade of toxodontids plus leontiniids.

Members of Oldfieldthomasiidae, Archaeopithecidae, and *Campanorco* are the earliest-diverging members of Typotheria in the unweighted analysis, with oldfieldthomasiids paraphyletic; the oldfieldthomasiid *Colbertia* forms a polytomy with: 1) a clade including *Oldfieldthomasia* as the sister group to a clade of the archaeopithecid *Acropithecus* and the campanorcid *Campanorco*; and 2) other typotheres. In the IW analysis, oldfieldthomasiids are polyphyletic, with *Oldfieldthomasia debilitata*, *Acropithecus rigidus*, and *Campanorco inauguralis* forming a sequentially diverging series of branches at the base of a clade formed by Mesotheriidae, Archaeohyracidae, and Hegetotheriidae, whereas *Colbertia magellanica* is the sister group to Interatheriidae (including a paraphyletic assemblage of taxa historically referred to as Notopithecinae or basal interatheriids as in Hitz et al. 2000, 2006). The unweighted analysis recovered Notopithecinae as a paraphyletic radiation at the base of Typotheria rather than

part of Interatheriidae; the IW analysis, however, recovered notopithecine taxa in a more conventional position (Hitz et al. 2000, 2006; Billet 2011), as a paraphyletic series of early diverging interatheriids. Other traditionally recognized groups of Typotheria are monophyletic, including Mesotheriidae, Archaeohyracidae, and Hegetotheriidae. Interatheriidae (exclusive of Notopithecinae in the unweighted analysis) is the sister group of a well-supported clade formed by Mesotheriidae and Hegetotheriidae + Archaeohyracidae, as suggested by some previous works (e.g., Cifelli 1993), but unlike the relationships recovered in some more recent phylogenies (e.g., Billet 2010, 2011).

A pruned phylogeny of taxa that are represented by endocasts, based on the unweighted analysis (Fig. 4a), is shown in Fig. 5 (see above). This phylogeny was also used as the framework for optimizations of endocranial traits (Table 4 and Fig. 6). This tree was further pruned for the tree-based PEQ analyses (see above; Fig. 7), as not all available casts provided enough information for an endocranial volume calculation. Therefore, *Oldfieldthomasia debilitata*, *Pachyrukhos moyani*, *Paedotherium bonaerense*, *Mesotherium cristatum*, and *Trachytherus alloxus* were excluded from the EQ analyses. One exception is *Interatherium robustum*, which was added to and included in the EQ analysis but was not included in the original pruned tree as we were not able to examine its endocast firsthand; Radinsky's (1981) description is not detailed enough to score endocranial characters in the phylogenetic matrix, but it does provide an estimate of endocranial volume for this species.

EQ Analysis

Notoungulates show relatively low EQs compared with modern mammals (Boddy et al. 2012), with the last common ancestor (LCA) of Notoungulata estimated as having an EQ of 0.5198 based on Jerison's equation (Fig. 7a). This low EQ is maintained in the early diverging notoungulate *N. murinus*, with slightly higher EQs in basal Toxodontia (*Rhyphodon* and *Homalodotherium*), although the relatively low EQs for this clade optimize as a secondary reduction because there is an ancestral increase in EQ at the Toxodontia + Typotheria node. EQ further increases in the toxodont lineage that includes *Leontinia* plus the clade of *Rhynchippus* + Toxodontidae. There are independent reversals to lower EQs in *Adinotherium* + *Nesodon* and in *Toxodon*. The highest EQ among notoungulates is found within Toxodontia, in *Leontinia*, with *Proadinotherium* also standing out among toxodontids due to its high EQ compared to other members of the family (Table 3 and Fig. 7a). At the base of Typotheria, there is an increase in EQ for the Hegetotheriidae + Mesotheriidae clade, with *Typotheriopsis* showing the highest EQ among typotheres (Fig. 7a). Interatheriids, on the other hand, show a reduction in EQ relative to the LCA of Typotheria + Toxodontia, with *Cochilius* showing a reduction to even lower EQ within the family and *Interatherium* optimizing as a slight increase relative to more basal interatheriid nodes.

PEQ results (Fig. 7b) are similar to EQ results using Jerison's (1973) equation, with an increase in PEQ in the LCA for Toxodontia + Typotheria, but noticeable reversals to lower PEQ values in *Rhyphodon*, *Homalodotherium*, and *Cochilius* (Fig. 7b). *Proadinotherium*, *Leontinia*, and *Rhynchippus* again stand out due to their exceptionally high PEQs. Interatheriids show a slight reduction in PEQ relative to the LCA of typotheres, with *Interatherium* reversing to a higher PEQ, while there is a tendency for a general increase in PEQ in the Hegetotheriidae + Mesotheriidae clade.

Discussion

Comparison of New Digital Endocasts of Notoungulata With Published Data From Near Relatives

Cochilius

Comparisons of the new digital endocasts of *Cochilius* sp. are made with previously described endocasts of other interatheriids— *Miocochilius anomopodus* (UCMP 39651 [Stirton 1953; Radinsky 1981]); species of *Protypotherium* (AMNH 9246 [Simpson 1933b; *Protypotherium* sp.]; FMNH P13002 [Radinsky 1981; *Pr. australe*]), and *Interatherium robustum* (FMNH P130547 [Radinsky 1981]).

A natural endocast of a Miocene interathere from Colombia, *Miocochilius anomopodus*, was described by Stirton (1953) with additional observations by Radinsky (1981). Distinctive features of this endocast that are similar to those of *Cochilius* include small olfactory bulbs relative to those of *Notostylops*, prominent endocast flexure, presence of a prominent Sylvian sulcus, exposure of only a shallow dimple marking the rostral portion of the median sulcus (i.e., longitudinal sulcus, medial longitudinal sulcus, central sulcus) that divides the right and left cerebral hemispheres, and no dorsal exposure of the midbrain (Stirton 1953; Radinsky 1981). *Miocochilius* differs from *Cochilius* in possessing a well-developed osseous tentorium, rounded paraflocculi, prominent anterior lobe of the cerebellum, and preservation of the pons on the ventral surface (Stirton 1953).

A partial artificial endocast extracted from a skull of *Protypotherium* sp. was described by Simpson (1933b); the olfactory bulbs, ventral surface, and occipital surface are partially or completely missing. This description was supplemented by Radinsky (1981) based on an additional endocast of *P. australe*. The dorsal surface of the cerebral hemisphere casts of *Protypotherium* is triangular in shape and shows that

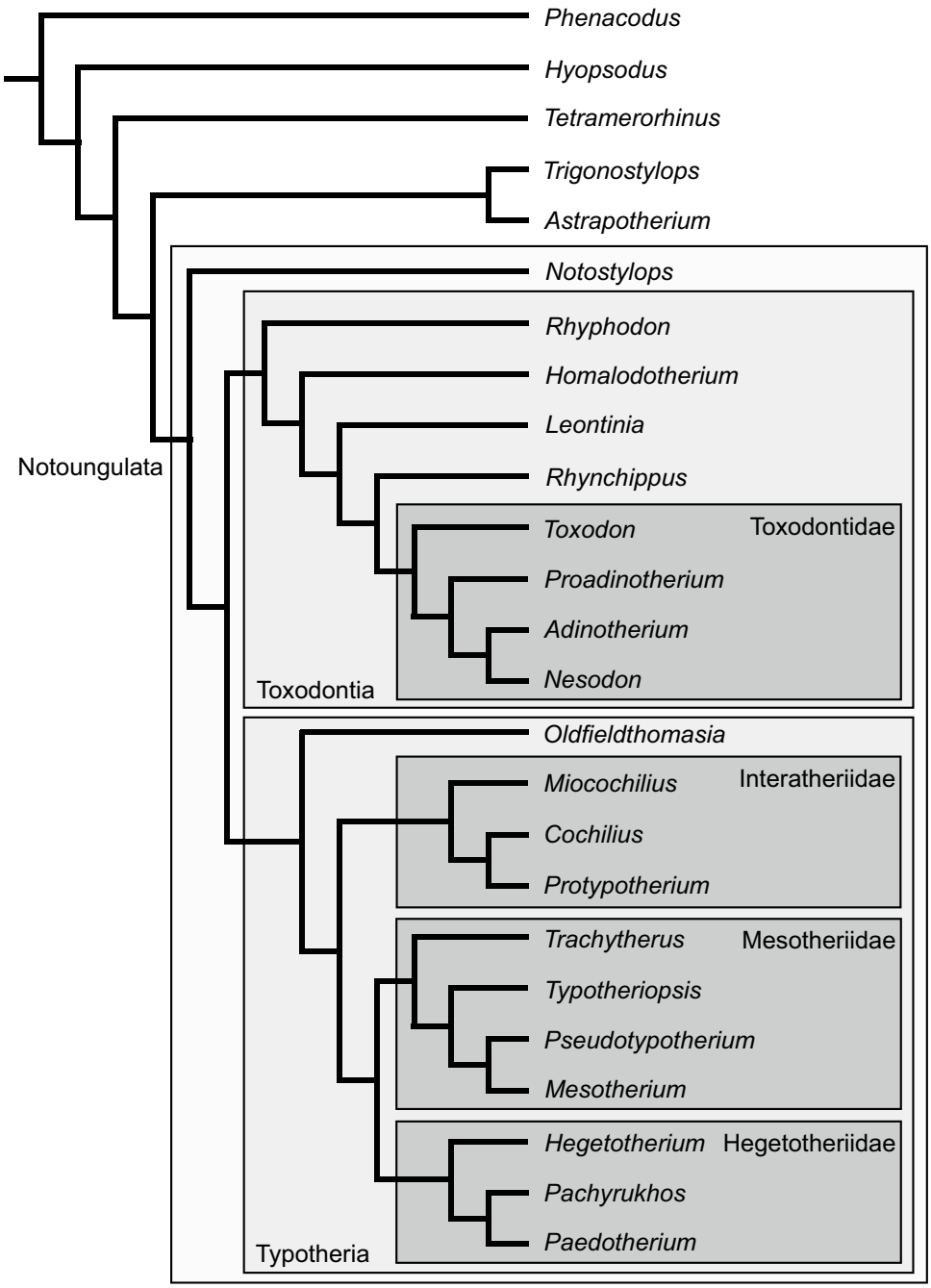

Fig. 5 Pruned tree (including only taxa with endocast data) of the Notoungulata phylogenies obtained here that was used in endocast character optimization analyses. Topology determined as explained in the text

the lateral sulcus, Sylvian sulcus, only the rostral portion of the median sulcus, and the lateral cerebral venous sinus in the cerebral region all are similar to *Cochilius* (Simpson 1933b; Radinsky 1981). The paraflocculi are cone-shaped in both *Protypotherium* and *Cochilius*. According to Simpson (1933b), the endocast of *Protypotherium* possesses a suprasylvian sulcus, unlike that of *Cochilius*.

An artificial endocast of another interathere, *Interatherium robustum*, was prepared by Radinsky (1981) to augment his description of the endocast of *Protypotherium*. Similar to *Protypotherium* and *Cochilius*, the dorsal surface of the cerebral hemisphere casts of *Interatherium* is triangular in shape, possesses a prominent Sylvian sulcus, and only the rostral portion of the median sulcus is visible (Radinsky 1981).

Notostylops

The digital endocast of the juvenile specimen of *N. murinus* described here closely compares to the endocast figures and descriptions of ontogenetically more advanced specimens of *Notostylops* described by Simpson (1932, 1933a). In

Table 4 Parsimony ancestral state reconstructions for endocast characters listed in Appendices 1 and 2, and Online Resources 1 and 2. Reconstructions and clade names are based on the pruned topology shown in Fig. 5

Character	Notoungulata	Toxodontia	Toxodontidae	Typotheria	Interatheriidae	Mesotheriidae	Hegetotheriidae
1	0	0	0	0	0	0	0
2	0	0	0/1	0	0	0	0/2
3	0	1	1	0	0	0	0
4	0	0	0	0	0	0	0
5	1	1	1	1	1	1	1
6	1	1	0	1	1	1	1
7	0	0	0	0	0	0	0
8	0	0	0	0	0	0	0
9	0	0/1	0	0	0	0	0
10	2	2	2	2	1	2	2
11	1	1	0/1	1	0/1	1	1
12	0	0	1	0	0	0	0
13	0	0	0	0	0	0	0
14	0	0	0	0	0	0	0
15	1	1	1	1	1	1	0
16	0	0	0	0	0	0	0
17	0/1	0/1	1	0/1	0/1	1	1
18	0	0	0	0	0	0	0
19	0	0	0	0	0	0	0
20	0	0	0	0	0	0	0
21	0	0	0	0	0	0	2
22	0/1	0	0/1	0	0	0	0

particular, the overall shape and proportions of the cerebral hemispheres, olfactory bulbs, and cerebellum of the digital endocast and older specimens are similar in dorsal and profile views (Fig. 3; Simpson 1932, 1933a). Even so, there are some differences that are discussed below.

Despite what Radinsky (1981:171) described as the "great exposure of the midbrain" on the endocast of *N. pendens* (originally described by Simpson 1933a), there are no impressions of midbrain structures on the skull roof bones and, consequently, no cast of any midbrain features on the dorsal surface of the digital endocast that we observed. Other mammalian endocasts displaying dorsal exposure of the midbrain preserve clearly delimited impressions of the colliculi (Bauchot and Stephan 1967). Meninges and the dural sinus system presumably filled in the space between the skull bones and the midbrain, as they do in many extant mammals, resulting in the smooth surface on the inferior surface of this portion of the parietals.

Simpson (1933a) described and figured an artificial endocast of *N. pendens* with a rhinal fissure, but Radinsky (1981) later questioned that interpretation. The new digital endocast of the specimen of *N. murinus* described here appears to show a rhinal fissure, supporting Simpson's original interpretation of rhinal fissure presence for *Notostylops*.

Endocast Character Optimizations

Ancestral character state reconstructions are presented in Table 4 for all 22 endocast characters listed in Appendix 1, and the optimizations of select characters are mapped onto the pruned phylogeny in Fig. 6. Character state 6.1 (presence of suprasylvian sulcus on cerebrum) optimizes as a synapomorphy of Notoungulata. Character state 2.1 (olfactory bulb wider than deep) and character state 3.1 (olfactory bulbs diverge from each other near their posterior junction with the rest of the cerebrum, just anterior to the circular fissure) are synapomorphies of Toxodontidae and Toxodontia, respectively. Two additional character states are equivocal synapomorphies for other clades of notoungulates: character states 10.1 (hypophyseal fossa width and length approximately equal) for Interatheriidae and 15.0 (paraflocculus cone-shaped) for Hegetotheriidae. Character 8 (separation of the anterior portion of the cavum epiptericum leading to the sphenorbital fissure) is invariant across our taxon sample but varies in other mammals (Macrini et al. 2007b) and may be phylogenetically informative at more inclusive taxonomic levels in future studies.

Multiple character states are autapomorphic within our taxonomic sample. Character state 4.1 (presence of a vascular foramen entering the olfactory bulb fossa) is only found in *Rhynchippus*, whereas character state 7.1 (presence of midbrain exposure on the dorsal surface of the endocast) is only found in *Hyopsodus*. Character states 16.1 (subarcuate fossa posterior to the internal auditory meatus) and 20.1 (absence of a separate optic fissure from cranial nerve II) are only found in *Rhyphodon*, and character state 18.1 (large recess dorsal to, and confluent with, canal leading to jugular foramen) is only exhibited in *Nesodon*. Character state 19.1 (foramen rotundum present; separate opening for V_2) is only seen in *Notostylops*.

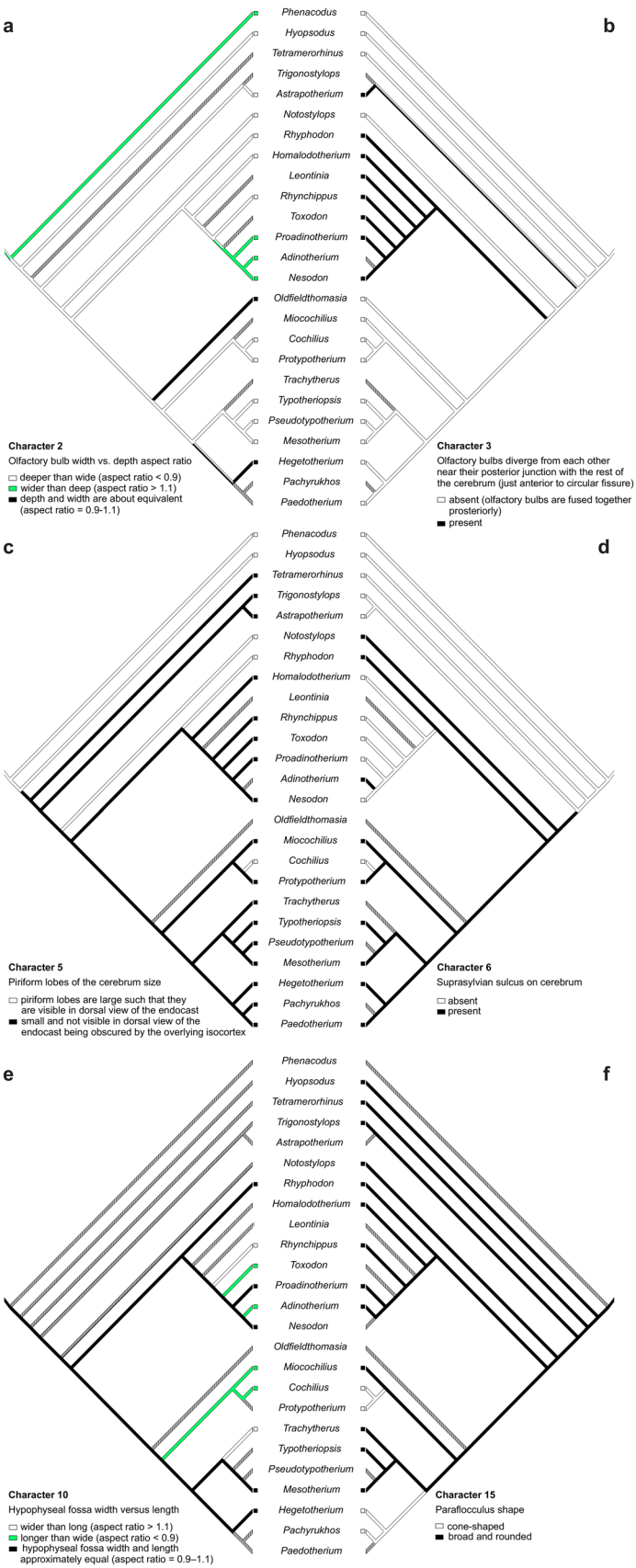

Fig. 6 Character transformations of six selected endocast characters (Appendix 1) based on DELTRAN optimization on the topology shown in Fig. 5. A striped branch leading to a terminal taxon indicates an unknown character state for that particular taxon

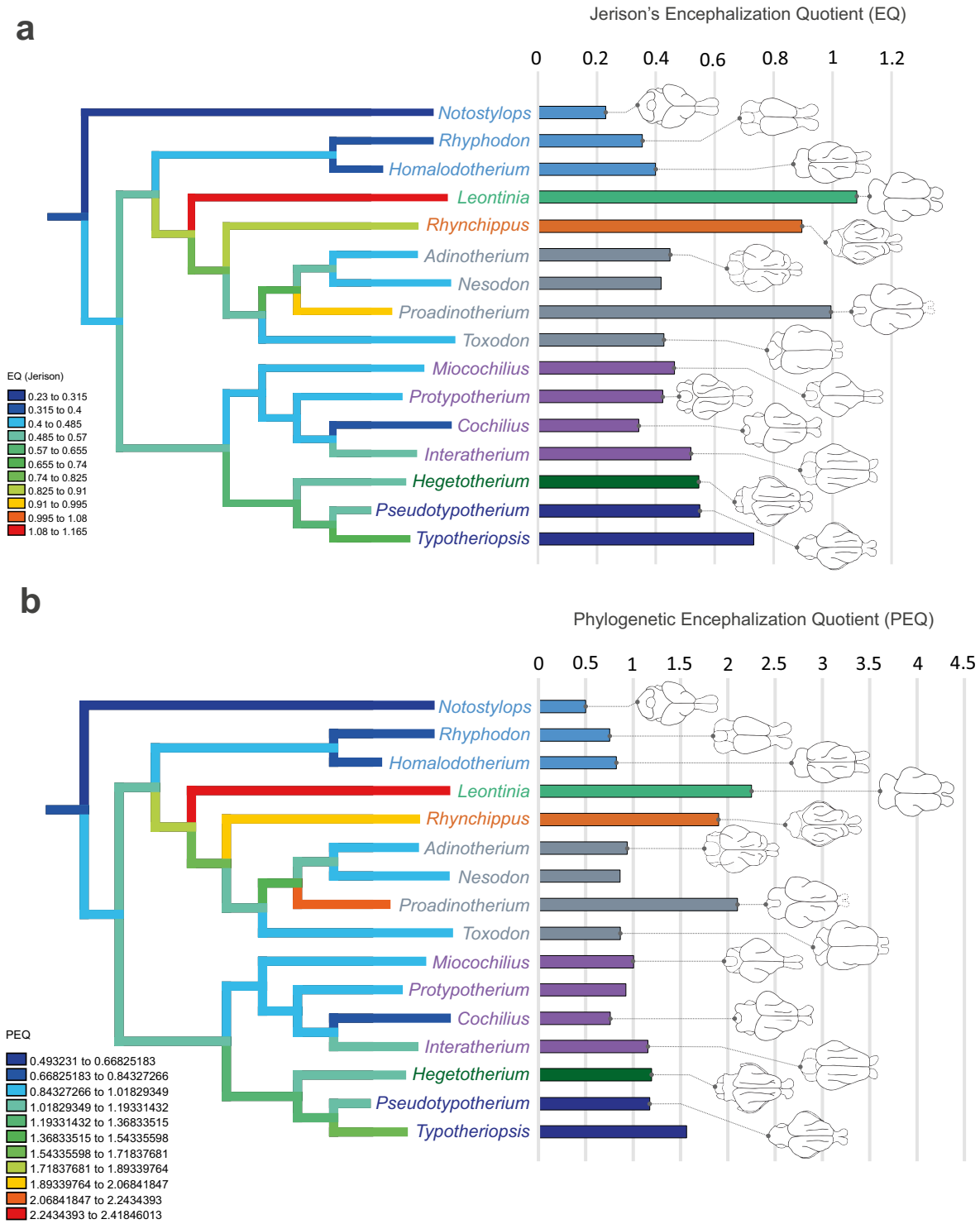

Fig. 7 Encephalization quotients (EQ) of notoungulate species with character transformations reconstructed using parsimony. The tree used is pruned from the trees obtained in Fig. 4. **a**, EQ calculated using Jerison's (1973) equation; **b**, EQ calculated using a Phylogenetic Encephalization Quotient (PEQ) corrected equation. Colors of branches (to the left of taxon names) correspond to binned ranges of EQs noted in the heat map explanation key for a-b. Colors of EQ bars (to the right of taxon names) correspond to families, with notoungulates of enigmatic or controversial relationships indicated by light blue; colors: light green, Leontiniidae; orange, "Notohippidae"; grey, Toxodontidae; purple, Interatheriidae; dark green, Hegetotheriidae; dark blue, Mesotheriidae

Nine endocast characters examined in this analysis do not vary for our sample and are not phylogenetically informative for the available taxonomic sample but may be useful at higher taxonomic levels and/or in larger taxonomic samples of notoungulates. The synapomorphies noted above and other character states showing phylogenetically informative and/or noteworthy distributions are described in more detail below.

Character state 2.1 (olfactory bulbs that are wider than deep) is a synapomorphy for Toxodontidae, as represented by *Proadinotherium muensteri*, *Nesodon imbricatus*, and *Adinotherium ovinum* (Fig. 6a). This character could not be scored for *Toxodon* sp. based on the endocast figures in Dechaseaux (1962). It also occurs convergently in the outgroup taxon *Phenacodus primaevus*.

Character state 3.1 (divergence of olfactory bulbs near their posterior junction with the rest of the cerebrum [just anterior to circular fissure]) is identified as a synapomorphy for Toxodontia as represented on endocasts of *Rhyphodon* sp., *Homalodotherium cunninghami*, *Leontinia gaudryi*, *Rhynchippus equinus*, *Toxodon* sp., *Proadinotherium muensteri*, and *Nesodon imbricatus* (Fig. 6b). The character state also is present independently in the outgroup *Astrapotherium magnum*.

Character state 10.1 (hypophyseal fossa that is longer than wide) is inferred to be a synapomorphy for Interatheriidae based on its presence in *Cochilius* and *Miocochilius*; the condition in *Protypotherium* is unknown (Fig. 6e). This character state also is observed independently in the toxodontids *Adinotherium* and *Toxodon,* while other toxodontids (*Proadinotherium, Nesodon*) retain the ancestral condition for toxodontians, Notoungulata, and nearest outgroups (Character state 10.2).

Character state 15.0 (cone-shaped parafloccular lobes of the cerebellum) represents a synapomorphy for hegetotheriids in our analysis, a feature convergent in some interatheriids (Fig. 6f). The hegetotheriids *Hegetotherium* and *Pachyrukhos* show this condition on their endocasts, but the condition is unknown in *Paedotherium*. This state is observed in the interatheriids *Cochilius* and *Protypotherium*, but the more basal interatheriid *Miocochilius anomopodus* exhibits character state 15.1 (broad and rounded parafloccular lobes), retaining the ancestral condition for notoungulates and nearest outgroups.

Of note, character state 5.1 (piriform lobes of the cerebrum small and not visible in dorsal view, being obscured by the overlying isocortex) is present in all notoungulates in this analysis for which this feature could be scored except for *Notostylops*, *Rhyphodon*, *Cochilius*, and *Mesotherium*. The condition is unknown in *Leontinia*, *Adinotherium*, and *Oldfieldthomasia*. This character state also is observed in the outgroups *Astrapotherium*, *Trigonostylops*, and *Tetramerorhinus*, and optimizes as ancestral for meridiungulates (Fig. 6c). The character state is convergent with the condition seen in members of several other placental groups (e.g., primates, cetaceans, proboscideans), some marsupials, and monotremes (Macrini 2006; Macrini et al. 2006; Rowe et al. 2011).

Also of note is character state 6.1 (suprasylvian sulcus present on cerebrum), which is mostly distributed in typotheres (*Miocochilius*, *Protypotherium*, *Hegetotherium*, *Paedotherium*, *Mesotherium*, and *Typotheriopsis*), but also is present in the toxodontians *Rhyphodon* and *Adinotherium* as well as in the basal notoungulate *Notostylops*; it optimizes as a synapomorphy of Notoungulata (Fig. 6d). However, most other toxodontians lack this sulcus, and its absence (a reversal from the ancestral condition for Notoungulata) optimizes as a synapomorphy of toxodontians exclusive of the earliest diverging *Rhyphodon*, with an independent reacquisition of the sulcus in *Adinotherium*. The suprasylvian sulcus also is absent independently in the typothere *Cochilius* (character state 6.0). The suprasylvian sulcus is also known on endocasts of other mammals such as artiodactyls (Macrini 2009).

Notoungulate Phylogenetic Relationships

In our analyses, there is support for a monophyletic Notoungulata (Fig. 4). The position of *N. murinus* is problematic and reminiscent of the results obtained by Billet (2010) that suggest that Pyrotheria belongs within Notoungulata (Billet 2010). Despite very different dentitions, there is some phylogenetic evidence that *Pyrotherium romeroi* may represent a highly divergent notoungulate, being particularly close to Notostylopidae in some analyses (Billet 2010, 2011). Our unweighted analysis (Fig. 4a) recovers *Py. romeroi* and *N. murinus* in a polytomy at the base of Notoungulata, together with *Carodnia vieirai*. The IW analysis (Fig. 4b), on the other hand, suggests that *Py. romeroi* (Pyrotheria) and *Ca. vieirai* (Xenungulata) are sister taxa, and that *N. murinus* is an early diverging taxon within a monophyletic Notoungulata. The dentition of *Ca. vieirai* does share some similarities with *Py. romeroi*, but the former taxon is still incompletely known, and the position of both xenungulates and pyrotheres has been highly contentious (Cifelli 1993; Agnolin and Chimento 2011; Kramarz and Bond 2014; Muizon et al. 2015; Croft et al. 2020). Similarities between the auditory region of *Py. romeroi* and notoungulates were noted by Patterson (1977), and the phylogeny of Billet (2010) gives some support for a close relationship. However, our results suggest that the phylogenetic position of Pyrotheria remains unresolved. *Notostylops murinus*, on the other hand, although sharing a basic cranial structure typical of notoungulates, is otherwise highly divergent in many features, as already noted by Simpson (1948), aggregating a great number of autapomorphies. This distinctiveness of Notostylopidae from other notoungulates and other meridiungulates, even

after inclusion of new endocranial data in our phylogenetic analyses, thus may continue to hinder disentanglement of its relationships.

Simpsonotus praecursor is one of the earliest well-known notoungulates (Pascual et al. 1978) and is frequently considered as one of the earliest diverging members of the clade (Billet 2011). This is supported by our IW analysis (Fig. 4b), although our unweighted analysis recovers it more deeply nested within Notoungulata, as an early offshoot of Toxodontia (Fig. 4a). The two traditionally recognized major subgroups of Notoungulata, Toxodontia and Typotheria (Cifelli 1993; Billet 2011), each are monophyletic and are sister taxa. Within Toxodontia, the results differ somewhat among our analyses. In the unweighted parsimony analysis (Fig. 4a), isotemnids form a paraphyletic assemblage at the base of a monophyletic clade composed of Homalodotheriidae, Leontiniidae, Notohippidae, and Toxodontidae, as suggested by Billet (2011). The IW analysis (Fig. 4b), however, recovers a monophyletic group composed of Isotemnidae. *Anisotemnus distentus* and *Thomashuxleya externa* are sister taxa in a polytomy with Toxodontia (inclusive of the henricosborniid *Simpsonotus* as its earliest diverging member) and Typotheria in the unweighted analysis (Fig. 4a) but are grouped with other Isotemnidae in the IW analysis (Fig. 4b). Isotemnidae is a group of early Cenozoic notoungulates almost universally thought to be non-monophyletic (Simpson 1948; Cifelli 1993; Billet 2011; see also Wyss et al. 2018). In contrast to that widespread presumption, and despite sharing many plesiomorphic characters, the results of our IW analysis suggest that at least some isotemnids may form a monophyletic clade (Fig. 4b). *Homalodotherium cunninghami* is sister group to a clade including Leontiniidae, Notohippidae, and Toxodontidae in the unweighted analysis (Fig. 4a), although Billet (2011), reaching the same results, acknowledged that only highly homoplastic characters support the position of Homalodotheriidae. In our analysis, five characters support this relationship, including an endocast character (Character 6; Fig. 6), but not one of them is unambiguous. The inclusion of Homalodotheriidae within Isotemnidae in our IW tree (Fig. 4b) is similar to the results obtained by Shockey et al. (2012) and is consistent with Cifelli's (1993) suggestion that homalodotheriids might be highly specialized isotemnids. Potential synapomorphies for a monophyletic Isotemnidae, including *H. cunninghami,* include a reduced-size i1 (character 94.2), which also appears independently in *Notostylops*, and at least two postcranial features: a well-developed supinator crest in the humerus (character 203.0), which is also a feature of some late-diverging typotheres such as mesotheriids, and a superior foramen in the astragalus (character 229.0), which also occurs in *Colbertia*. However, as this latter character state is the primitive condition for therians (Meng et al. 2003) and has been lost independently in many groups of placental mammals, including many notoungulates (Horovitz 2000; Shockey and Flynn 2007; Vera 2012; Croft and Lorente 2021), it is more likely a symplesiomorphy despite its optimization in our analysis. As many notoungulates and other Paleogene South American native ungulates still lack adequately known postcranial remains, the status of these character states as synapomorphies should be considered provisional. One endocast character, a sphenorbital fissure even with or just behind the circular fissure (character 9.1), may also be a synapomorphy of this clade.

The grouping of Leontiniidae, Toxodontidae, and Notohippidae in a monophyletic clade has long been recognized (e.g., Cifelli 1993; Billet 2011; Shockey et al. 2012). Leontiniidae (exclusive of *Colpodon*; see below) and Toxodontidae are monophyletic, but notohippids, as seems to be well established (Cifelli 1993; Shockey 1997; Cerdeño and Vera 2017; Billet 2011; Shockey et al. 2012; see also Wyss et al. 2018), form a paraphyletic array of taxa at the base of Toxodontidae in both analyses (Fig. 4a, b). Of particular interest is the position of *Colpodon propinquus*, which is traditionally considered a member of Leontiniidae but also shares many characteristics with Toxodontidae and Notohippidae (Cifelli 1993). In our analyses, *Co. propinquus* was consistently recovered at the base of the clade of Notohippidae + Toxodontidae. At least one synapomorphy supports this relationship unambiguously, a crista intermedia running lingually from the ectoloph between the protoloph and the crochet on upper cheek teeth (character 47.0), but the discovery of new characters and additional analyses may be necessary to test among these competing hypotheses of relationships for *Colpodon*.

Members of three families in our analyses, Oldfieldthomasiidae (represented by *Colbertia* and *Oldfieldthomasia*), Archaeopithecidae (*Acropithecus*), and "Campanorcidae" (*Campanorco inauguralis*) (García-López and Babot 2017), are poorly known taxa that usually have unstable positions in phylogenetic analyses (Cifelli 1993); they also have differing interrelationships in our two analyses, although they are members of Typotheria in both (Fig. 4a, b), and are usually assumed to be paraphyletic (e.g., Billet 2011; García-López and Babot 2015). Oldfieldthomasiidae is not clearly monophyletic in our analyses, with its two species either divided between interatheriids and remaining typotheres (Fig. 4b) or in a polytomy at the base of Typotheria (Fig. 4a, with *Oldfieldthomasia* linked to a clade of *Acropithecus* + *Campanorco*). *Campanorco inauguralis* remains an enigmatic taxon, frequently recovered in a polytomy at the base of Typotheria (Billet 2011), as in our unweighted analysis (Fig. 4a), but also sometimes considered an early member of the clade including Mesotheriidae, Archaeohyracidae, and Hegetotheriidae (Reguero and Prevosti 2010), a position supported by our IW analysis (Fig. 4b).

Results for Typotheria suggest the monophyly of most families, including Archaeohyracidae, Hegetotheriidae,

Mesotheriidae, and at least interatheriine Interatheriidae (unweighted analysis; Fig. 4a), but also probably all of Interatheriidae (IW analysis; Fig. 4b). The position of Mesotheriidae as sister group of Hegetotheriidae + Archaeohyracidae was recovered in both analyses (Fig. 4a, b) and agrees with most prior phylogenies (Cifelli 1993; Croft et al. 2003; Billet et al. 2009; Reguero and Prevosti 2010), although monophyly of Archaeohyracidae has been contested in the past (Croft et al. 2003; Billet et al. 2009). Phylogenetic relationships among species of 'Notopithecinae' or basal interatheriids are rarely addressed, with many phylogenies including only a single member of the subfamily (Reguero et al. 2003; Billet 2011). In most studies analyzing numerous 'notopithecines', however, they are considered a paraphyletic assemblage of early diverging Interatheriidae (Hitz et al. 2006), although other studies recover some 'notopithecines' as a monophyletic group of basal interatheriids (Vera 2016). Our IW analysis supports a monophyletic Interatheriidae, with Interatheriinae nested within the paraphyletic 'Notopithecinae' (Fig. 4b), a commonly shared view (Hitz et al. 2006). Our unweighted analysis (Fig. 4a), however, recovers 'notopithecine' taxa as not closely related to Interatheriinae (and thus not interatheriids), instead forming a paraphyletic radiation at the base of Typotheria. Additional studies with even more comprehensive taxonomic and character sampling will permit testing of these alternative hypotheses of 'notopithecine' relationships as well as other points of uncertainty in our phylogeny, such as some unresolved relationships within Toxodontia. The inclusion of early diverging taxa within each group, in particular, may alter the relationships presented here.

Evolution of Encephalization in Notoungulates

The mean Encephalization Quotient (EQ) among notoungulates evaluated in this study is low compared to living mammals with presumably similar habits (Fig. 7a and Table 3), being 0.55 (using Eisenberg's (1981) equation) or 0.52 (using Jerison's (1973) equation). Mean EQ values for notoungulates are well below extant ungulates, such as perissodactyls (1.0) and artiodactyls (minus Cetacea; 1.42), and even lower than dominantly smaller bodied and herbivorous rodents (0.6; Boddy et al. 2012). Body mass estimates, especially in extinct taxa like notoungulates without close living analogs, can be challenging. Prior authors (e.g., Jerison 1973; Radinsky 1981; Cassini et al. 2012a, b; Elissamburu 2012) have provided widely varying estimates, and this can result in markedly divergent EQs. We provide justifications of our body mass estimates in Online Resource 3 but acknowledge that using different estimates could alter some of the conclusions reached here and that this issue should always be carefully considered in studies that reach conclusions based on indirect data in extinct species.

Many factors are thought to influence EQ in mammals. Relatively small brains may reflect maintenance of the ancestral condition because early mammals tended to have relatively low EQs in comparison with later diverging forms (Jerison 1973). However, as divergence or phylogenesis continues, patterns of encephalization within groups tend also to become more complex (Schultz and Dunbar 2010), and EQ starts to vary widely in response to other factors. At this point, purely directional explanations are not sufficient to explain variation in EQ within some groups, as other factors come into play.

One of the factors that may influence brain size is the large energetic expenditure of this organ, which may be especially metabolically costly for large bodied mammals since larger bodies also imply an increase in energetic requirements (Marquet and Taper 1998). This relationship may be particularly relevant for large bodied notoungulate groups, such as the Toxodontia. Without evolutionary pressures to maintain large brains, brain reduction may occur in some large bodied mammals, especially those with other metabolically expensive organs and tissues, such as the large and complex guts of herbivores (Striedter 2005; Boddy et al. 2012).

However, one of the most common explanations for the low EQ of notoungulates is brain reduction due to insularism. It is well known that some mammal lineages may undergo brain size reduction when evolving under isolated conditions (van der Geer et al. 2010), which is usually attributed to reduction of predation pressure and low competition in island ecosystems. Low levels of predation also have been proposed to drive decline in EQ under other circumstances, such as reduced selection due to the evolution of antipredator defenses (Stankowich and Romero 2017).

Because South America was an isolated continent during most of the Cenozoic, notoungulates were predated upon by relatively few, generally small brained metatherians and non-mammalian predators (Croft 2001, 2006), which may account for relatively small brains of notoungulates compared to mammals on other continents (Jerison 1973; Fernández-Monescillo et al. 2019). The phenomenon of brain reduction in large bodied South American herbivorous mammals is well documented. Some neoepiblemid rodents, which achieved large body sizes and may have shared some of the large bodied herbivorous mammal ecological niches with various larger bodied notoungulates, show remarkably low EQs when compared with other rodents and similarly sized mammals, and this also has been attributed to lower predation pressures (Ferreira et al. 2020). However, it has been argued that predator guilds in Cenozoic South America were not particularly impoverished compared to other continents based on studies of an early Miocene ecological community of Patagonia (Kay et al. 2012; Rodríguez-Gómez et al. 2020). In either case, metatherian predators may be subject to intrinsic ecological and evolutionary limitations (Croft et al.

2018), which could include less developed brain and cognitive abilities, implying reduced pressure on their prey.

In spite of the overall generally low EQ of notoungulates relative to ecologically comparable herbivores on other continents, substantial variations in EQ can be detected along branches of the Notoungulata tree, including both clade-specific changes and independent increases or decreases (Fig. 7). Both traditional EQ analyses and PEQ yield similar results, with a very low EQ and PEQ for the LCA of Notoungulata, and relatively low EQs/PEQs ancestrally in early diverging toxodontians, most toxodontids, and interatheriid typotheres, with *Cochilius* in particular showing a substantial secondary reduction in EQ/PEQ within interatheriids. Notable increases in EQ and PEQ occur in the LCA of leontiniids + notohippids + toxodontids, with a further independent increase in *Leontinia*, *Rhynchippus*, and *Proadinotherium* among toxodontians, and in the LCA of hegetotheriids + mesotheriids among typotheres.

Fernández-Monescillo et al. (2019) found that mesotheriids displayed relatively low EQ values compared with other notoungulates, which was attributed to their semifossorial habits. In contrast, the two mesotheriids evaluated in our study (*Pseudotypotherium* and *Typotheriopsis*) show relatively high EQs and PEQs compared to other notoungulates (Fig. 7 and Table 3). The notoungulate EQ values found by Fernández-Monescillo et al. (2019), as well as the EQ values of notohippids and leontiniids of Dozo and Martínez (2016) and Martínez et al. (2019), generally are lower than those found here, likely due to differences in estimation of body mass (see above).

On the other hand, there are some instances of marked increases in EQ/PEQ among notoungulates (Fig. 7). *Proadinotherium* is one of the smallest toxodontids, with an estimated weight around 40 kg (Radinsky 1981), but it has the highest EQ/PEQ in the family and one of the highest among notoungulates. The notohippid *Rhynchippus* and the leontiniid *Leontinia* also show higher EQs/PEQs than most notoungulates, with *Leontinia* in particular having the highest EQ/PEQ among all notoungulates sampled. Toxodontians and typotheres together show an increase in EQ/PEQ relative to the ancestral notoungulate condition. The sampled species of typotheres maintain relatively homogeneous EQs/PEQs overall but with a substantial secondary decrease in EQ/PEQ in the interatheriid *Cochilius* and an increase in the mesotheriid + hegetotheriid clade, with the mesotheriid *Typotheriopsis* showing a particularly noticeable increase in EQ/PEQ (Fig. 7). Among toxodontians, higher EQs/PEQs seem to be associated with smaller bodied taxa, even though these measures already standardize for body size, with the notable exception of the large-bodied *Leontinia*. Increased brain size is more commonly associated with more complex social behavior (Dunbar 1995; Striedter 2005; Schultz and Dunbar 2010), and the results herein are consistent with inferences of gregarious behavior in these species. However, many additional factors may be involved in brain size evolution in mammals, especially in species with such distinctive histories as the endemic South American 'ungulates', and it remains to be further tested to determine if the broad conclusions of this study remain supported when additional taxa are sampled.

Little is still known about social behavior in notoungulates and possible consequences of brain structure for specific cognitive abilities among extinct South American ungulates. This may represent an area ripe for future investigation of patterns in evolution of particular brain regions that clearly are associated with particular cognitive functions in extant mammals. There still is but a small sample notoungulate endocasts available relative to the rich species diversity in the group, which can be seen by comparing our pruned tree with the sampling in the full phylogenetic analyses. As our knowledge of the brain morphology and encephalization of notoungulates increases, primarily as CT scanning makes comparative data more readily available, we expect to continue to expand knowledge of the brain anatomy, sensory capabilities and cognition of notoungulates.

Appendix 1—Cranial endocast characters. Complete list of characters is presented in Online Resource 1

1. Olfactory bulb width vs. length aspect ratio: longer than wide (aspect ratio < 0.9) (0), wider than long (aspect ratio > 1.1) (1), or length and width are about equivalent (aspect ratio = 0.9–1.1) (2) (Macrini 2006: character #9). Aspect ratios rounded to nearest 0.1; see Fig. 1 for illustration of measurements.
2. Olfactory bulb width vs. depth aspect ratio: deeper than wide (aspect ratio < 0.9) (0), wider than deep (aspect ratio > 1.1) (1), or depth and width are about equivalent (aspect ratio = 0.9–1.1) (2). **New character.** Aspect ratios rounded to nearest 0.1; see Fig. 1 for illustration of measurements.
3. Olfactory bulbs diverge from each other near their posterior junction with the rest of the cerebrum (just anterior to circular fissure): absent (olfactory bulbs are fused together posteriorly) (0), or present (1). **New character.**
4. Vascular foramen entering the olfactory bulb fossa: absent (0), or present (1). **New character.** This character was scored from original CT data or illustrations by Patterson (1937), Simpson (1933a, b), and Stirton (1953).

5. Piriform lobes of the cerebrum size: large, such that they are visible in dorsal view of the endocast (0), small, not visible in dorsal view of the endocast being obscured by the overlying isocortex (1). **New character.**
6. Suprasylvian sulcus on cerebrum: absent (0), or present (1). **New character.**
7. Midbrain exposure on the dorsal surface of the endocast: absent (0), or present (1) (Macrini et al. 2007b: character #11).
8. Anterior portion of cavum epiptericum leading to the sphenorbital fissure: anterior portions of right and left cava are at least partially separated at sphenorbital fissure (0), cava are completely confluent at sphenorbital fissure (1) (Macrini et al. 2007b: character #21).
9. Sphenorbital fissure position: located well behind the circular fissure (0), even with or just behind the circular fissure (1). **New character.**
10. Hypophyseal fossa width versus length: wider than long (aspect ratio > 1.1) (0), longer than wide (aspect ratio < 0.9) (1), width and length approximately equal (aspect ratio = 0.9–1.1) (2) (Macrini et al. 2007b: character #18). Aspect ratios rounded to nearest 0.1; see Fig. 1 for illustration of measurements.
11. Hypophysis depth: deep, extending well below the anterior portion of the cavum epiptericum leading to the sphenorbital fissure (0), shallow, lying dorsal or even with the anterior cavum epiptericum (1). See Fig. 1 for illustration of measurement. **New character**.
12. Posterior clinoid process of the dorsum sellae: absent (does not leave an impression on the endocast) (0), concavity present (1), narrow ridge present, extending from clinoid process (2). **New character**.
13. Pons: absent (0), present (1) (Macrini 2006: character #23). An impression of the pons is not clearly visible on most mammalian endocasts because the meninges and cisterns (i.e., expansive subarachnoid spaces filled with cerebrospinal fluid) in this area fill in the space surrounding and lying between the brain and basicranial bones. It is unclear if those taxa with a pons exposed on their endocast have a particularly large pons relative to the meninges and cisterns, or if meninges and cisterns instead are particularly thin and small in this area.
14. Paraflocculus of cerebellum: present (0), absent (1) (Macrini et al. 2007b: character #15; character reworded).
15. Paraflocculus shape: cone-shaped (0), broad and rounded (1) (modified from Macrini et al. 2007b: character #16).
16. Subarcuate fossa position relative to internal auditory meatus (IAM): subarcuate fossa dorsal or posterodorsal to IAM (0), subarcuate fossa posterior to IAM (1) (modified from Gabbert 1997: character #17).
17. Lateral cerebral venous sinus: absent (0), present (1). **New character**.
18. Large recess dorsal to, and confluent with, canal leading to jugular foramen: absent (0), present (1). This recess may house the lateral sinus. **New character**.
19. Foramen rotundum (separate opening for V_2): absent (0), present (1) (Geisler and Uhen 2003: character #50).
20. Optic fissure (cranial nerve II opening separate from sphenorbital fissure): present (0), absent (1) (modified from Macrini 2006: character #39).
21. Endocranial flexure: slight or no flexure (0), flexed with cerebrum inclined anterodorsally when medulla is oriented horizontally (1), flexed with cerebrum inclined anteroventrally when medulla is oriented horizontally (2). **New character**.
22. Osseous tentorium: absent (0), present and represented by posteromedial ossification of tentorium cerebelli (1), present as a lateral ossification of tentorium cerebelli (2) (modified from Macrini et al. 2007b: character #10). We scored this character by inferring the morphology of the osseous tentorium from endocasts, but this also can also be scored via direct observation of a bony tentorium.

Appendix 2—Taxon x cranial endocast character matrix. Complete phylogenetic matrix is presented in Online Resource 2

Taxon	1	2	3	4	5	6	7	8	9	10	11	12	13	14	15	16	17	18	19	20	21	22
Adinotherium	1	1	?	?	?	1	0	0	0	1	1	0	0	0	1	0	1	0	?	0	2	1
Proadinotherium	1	1	1	?	1	0	0	0	0	2	0	1	1	0	1	0	0	0	0	0	2	0
Nesodon	2	1	1	0	1	0	0	0	0	2	0	2	0	1	N	N	1	1	0	0	1	1
Rhynchippus	0	0	1	1	1	0	0	0	0	0	0	1	0	0	1	0	1	0	0	0	0	0
Homalodotherium	0	0	1	0	1	0	0	0	1	?	?	?	0	0	1	0	1	0	0	0	2	1
Rhyphodon	0	0	1	0	0	1	0	0	1	2	1	0	0	0	1	1	0	0	0	1	0	0
Oldfieldthomasia	0	2	0	?	?	?	?	?	?	?	?	?	?	?	?	?	?	?	?	?	?	?
Hegetotherium	0	2	0	0	1	1	0	0	0	2	1	0	0	0	0	0	1	0	0	0	2	0
Paedotherium	?	?	0	?	1	1	0	?	?	?	?	?	?	?	?	?	1	?	?	?	?	?
Typotheriopsis	0	0	0	0	1	1	0	?	?	?	?	?	?	0	1	0	1	?	?	?	0	2
Protypotherium	2	0	0	?	1	1	0	?	?	?	?	?	?	0	0	0	1	?	?	?	?	2
Miocochilius	0	?	0	0	1	1	0	0	0	1	?	0	1	0	1	0	0	0	0	0	0	0
Cochilius	0	0	0	0	0	0	0	0	0	1	0	0	0	0	0	0	1	0	0	0	0	0
Notostylops	0	0	0	0	0	1	0	0	0	?	?	0	0	0	1	0	0	0	1	0	0	1
Toxodon	0	?	1	?	1	0	0	0	0	1	1	1	?	1	N	N	?	?	0	0	0	1
Leontinia	1	?	1	?	?	?	0	?	?	?	?	?	?	1	N	N	?	?	?	?	?	0
Pachyrukhos	?	?	?	?	1	?	?	?	?	?	?	?	?	0	0	0	?	?	?	?	2	?
Mesotherium	0	0	0	0	1	1	0	0	0	2	0	0	?	0	1	0	0	0	0	0	2	1
Pseudotypotherium	1	0	0	0	1	?	0	?	?	?	0	?	?	?	?	?	1	0	?	?	0	0
Trachytherus	?	?	?	?	1	?	?	0	0	0	1	0	?	0	1	0	?	?	0	0	0	?
Tetramerorhinus	?	?	0	?	1	0	0	0	0	?	?	?	?	0	1	0	1	0	0	0	2	0
Trigonostylops	?	?	?	?	1	0	0	0	0	?	?	?	?	0	1	0	1	?	?	0	0	1
Astrapotherium	0	0	1	0	1	0	0	?	?	?	?	?	?	1	N	N	0	?	?	?	0	0
Phenacodus	2	1	0	0	0	0	0	0	0	?	1	1	1	1	N	N	0	0	0	0	2	1
Hyopsodus	0	0	0	0	0	0	1	0	0	?	?	?	0	0	1	0	0	0	0	0	0	1

Character data sources—direct specimen observation, illustrations, or literature descriptions of specimens: *Adinotherium* (AMNH 55969; Patterson 1937; Radinsky 1981); *Proadinotherium* (AMNH 55970; Radinsky 1981); *Nesodon* (FMNH P13076; Patterson 1937; Radinsky 1981); *Rhynchippus* (FMNH P13420; Patterson 1937); *Homalodotherium* (FMNH P13092; Patterson 1937); *Rhyphodon* (AMNH 29414; Simpson 1933a); *Oldfieldthomasia* (AMNH 28780; Simpson 1932); *Hegetotherium* (AMNH 9223; Simpson 1933b); *Paedotherium* (AMNH 45914; Radinsky 1981; Dozo 1997); *Typotheriopsis* (FMNH P14420; Patterson 1937); *Protypotherium* (AMNH 9246; Simpson 1933b; Radinsky 1981); *Miocochilius* (Stirton 1953; Radinsky 1981); *Cochilius* (SGOPV 3774; This Study); *Notostylops* (FMNH P13319; AMNH 28614; This Study; Simpson 1932, 1933a); *Toxodon* (Dechaseaux 1962); *Leontinia* (Radinsky 1981); *Pachyrukhos* (AMNH 9525; AMNH 15918; Dechaseaux 1962; Radinsky 1981); *Mesotherium* (Dechaseaux 1962); *Pseudotypotherium* (Radinsky 1981); *Trachytherus* (Patterson 1934); *Tetramerorhinus* (AMNH 9245; Simpson 1933b); *Trigonostylops* (AMNH 28700); *Astrapotherium* (AMNH 55968; Radinsky 1981); *Phenacodus* (Simpson 1933a); *Hyopsodus* (Orliac et al. 2012)

?, unknown; **N**, not applicable

Supplementary Information The online version contains supplementary material available at https://doi.org/10.1007/s10914-021-09583-4.

Acknowledgments We thank Tim Ryan (Department of Anthropology; Center for Quantitative X-ray Imaging at Penn State University) for scanning of the specimens. Funding was provided by NSF DEB-0513476 to JJF and a Frick Postdoctoral Fellowship (2008-09) from the Department of Vertebrate Paleontology (Division of Paleontology) at the AMNH to TEM. This work also represents a contribution to the AToL-Mammal Morphology studies supported by BIO EF- 0629811 (to JFF and colleagues). FAP was funded by the National Council for Scientific and Technological Development – CNPq (422868/2016-7). We thank Julio C. La Torre, who was funded by an NSF REU to AMNH, for assistance with scoring the cranial endocast characters, and Daniel M. Casali for comments on an early version of the manuscript. We also extend our appreciation to Guillaume Billet and an anonymous reviewer for their thoughtful and helpful comments and suggestions which improved the manuscript.

References

Agnolin FL, Chimento NR (2011) Afrotherian affinities for endemic South American ungulates. Mammal Biol 76:101-108. https://doi.org/10.1016/j.mambio.2010.12.001

Bauchot R, Stephan H (1967) Encéphales et moulages endocraniens de quelques insectivores et primates actuels. In: Lehman J-P (ed) Problèmes actuels de paléontologie (Évolution des Vertébrés): Colloques Internationaux du Centre National de la Recherche Scientifique. Éditions du centre national de la recherche scientifique, Paris, pp 575-586

Billet G (2010) New observations on the skull of *Pyrotherium* (Pyrotheria, Mammalia) and new phylogenetic hypotheses on South American ungulates. J Mammal Evol 17:21-59. https://doi.org/10.1007/s10914-009-9123-0

Billet G (2011) Phylogeny of the Notoungulata (Mammalia) based on cranial and dental characters. J Syst Palaeontol 9:481-497. https://doi.org/10.1080/14772019.2010.528456

Billet G, Martin T (2011) No evidence for an afrotherian-like delayed dental eruption in South American notoungulates. Naturwissenschaften 98:509-517. https://doi.org/10.1007/s00114-011-0795-y

Billet G, Muizon C de (2013) External and internal anatomy of a petrosal from the late Paleocene of Itaboraí, Brazil, referred to Notoungulata (*Placentalia*). J Vertebr Paleont 33:455-469. https://doi.org/10.1080/02724634.2013.722153

Billet G, Patterson B, Muizon C de (2009) Craniodental anatomy of late Oligocene archaeohyracids (Notoungulata, Mammalia) from Bolivia and Argentina and new phylogenetic hypotheses. Zool J Linnean Soc 155:458-509. https://doi.org/10.1111/j.1096-3642.2008.00445.x

Billet G, Hautier L, Lebrun R (2015a) Morphological diversity of the bony labyrinth (inner ear) in extant xenarthrans and its relation to phylogeny. J Mammal 96:658-672. https://doi.org/10.1093/jmammal/gyv074

Billet G, Muizon C, de Schellhorn R, Ruf I, Ladevèze S, Bergqvist L (2015b) Petrosal and inner ear anatomy and allometry amongst specimens referred to Litopterna (*Placentalia*). Zool J Linnean Soc 173:956-987. https://doi.org/10.1111/zoj.12219

Boddy AM, McGowen MR, Sherwood CC, Grossman LI, Goodman M, Wildman DE (2012) Comparative analysis of encephalization in mammals reveals relaxed constraints on anthropoid primate and cetacean brain scaling. J Evol Biol 25:981-994. https://doi.org/10.1111/j.1420-9101.2012.02491.x

Bremer K (1994) Branch support and tree stability. Cladistics 10:295-304. https://doi.org/10.1006/clad.1994.1019

Buckley M (2015) Ancient collagen reveals evolutionary history of the endemic South American ungulates. Proc R Soc B 282:20142671. https://doi.org/10.1098/rspb.2014.2671

Cassini GH, Vizcaíno SF, Bargo MS (2012a) Body mass estimation in early Miocene native South American ungulates: a predictive equation based on 3D landmarks. J Zool 287:53-64. https://doi.org/10.1111/j.1469-7998.2011.00886.x

Cassini GH, Cerdeño E, Villafañe AL, Muñoz NA (2012b) Paleobiology of Santacrucian native ungulates (Meridiungulata; Astrapotheria, Litopterna and Notoungulata). In Vizcaíno SF, Kay RF, Bargo MS (eds) Early Miocene Paleobiology in Patagonia: High-Latitude Paleocommunities of the Santa Cruz Formation. Cambridge University Press, Cambridge, pp 243–286. https://doi.org/10.1017/CBO9780511667381.015

Cerdeño E, Bond M (1998) Taxonomic revision and phylogeny of *Paedotherium* and *Tremacyllus* (Pachyrukhinae, Hegetotheriidae, Notoungulata) from the late Miocene to Pleistocene of Argentina. J Vertebr Paleontol 18:799-811. https://doi.org/10.1080/02724634.1998.10011108

Cerdeño E, Vera B (2017) New Anatomical Data on *Pyrotherium* (Pyrotheriidae) from the Late Oligocene of Mendoza Argentina. Ameghiniana 54:290-306. https://doi.org/10.5710/AMGH.14.11.2016.3052

Cifelli RL (1985) Biostratigraphy of the Casamayoran, early Eocene, of Patagonia. Am Mus Novitates 2820:1-26.

Cifelli RL (1993) The phylogeny of the native South American ungulates. In: Szalay FS, Novacek MJ, McKenna MC (eds) Mammal Phylogeny. Volume 2: Placentals. Springer-Verlag, New York, pp 195-216

Croft DA (2000) Archaeohyracidae (Mammalia: Notoungulata) from the Tinguiririca fauna, central Chile, and the evolution and paleoecology of South American mammalian herbivores. Dissertation, University of Chicago, Chicago

Croft DA (2001) Cenozoic environmental change in South America as indicated by mammalian body size distributions (cenograms). Divers Distrib 7:271-287. https://doi.org/10.1046/j.1366-9516.2001.00117.x

Croft DA (2006) Do marsupials make good predators? Insights from predator-prey diversity ratios. Evol Ecol Res 8:1193-1214.

Croft DA (2016) Horned Armadillos and Rafting Monkeys: The Fascinating Fossil Mammals of South America. Indiana University Press, Bloomington

Croft DA, Anaya F (2006) A new middle Miocene hegetotheriid (Notoungulata: Typotheria) and a phylogeny of the Hegetotheriidae. J Vertebr Paleontol 26:387-399. https://doi.org/10.1671/0272-4634(2006)26[387:ANMMHN]2.0.CO;2

Croft DA, Lorente M (2021) No evidence for parallel evolution of cursorial limb adaptations among Neogene South American native ungulates (SANUs). PLoS One 16:e0256371. https://doi.org/10.1371/journal.pone.0256371

Croft DA, Bond M, Flynn JJ, Reguero MA, Wyss AR (2003) Large archaeohyracids (Typotheria, Notoungulata) from central Chile and Patagonia, including a revision of *Archaeotypotherium*. Fieldiana Geol (New Series) 49:1-38. https://doi.org/10.5962/bhl.title.5264

Croft DA, Engelman RK, Dolgushina T, Wesley G (2018) Diversity and disparity of sparassodonts (Metatheria) reveal non-analogue nature of ancient South American mammalian carnivore guilds. Proc Biol Sci B Biol Sci 285:20172012. https://doi.org/10.1098/rspb.2017.2012

Croft DA, Flynn JJ, Wyss AR (2004) Notoungulata and Litopterna of the early Miocene Chucal fauna, northern Chile. Fieldiana Geol (New Series) 50:1-52. https://doi.org/10.3158/0096-2651(2004)50/1:NALOTE/2.0.CO;2

Croft DA, Gelfo JN, López GM (2020) Splendid innovation: the South American native ungulates. Annu Rev Earth Planet Sci 48:259-290. https://doi.org/10.1146/annurev-earth-072619-060126

Dechaseaux C (1958) Encéphale de Litopternes, encéphales de Notoungulés. In: Piveteau J (ed) Traité de Paléontologie, Tome VI, Volume 2. Masson, Paris, pp 58–59, 121–129

Dechaseaux C (1962) Encéfalos de notoungulados y de desdentados xenartros fósiles. Ameghiniana 2:193-209

Dozo MT (1997) Paleoneurología de *Dolicavia minuscula* (Rodentia, Caviidae) y *Paedotherium insigne* (Notoungulata, Hegetotheriidae) del Plioceno de Buenos Aires, Argentina. Ameghiniana 34:427-435

Dozo MT, Martínez G (2016) First digital cranial endocasts of late Oligocene Notohippidae (Notoungulata): implications for endemic South American ungulate brain evolution. J Mammal Evol 23:1-16. https://doi.org/10.1007/s10914-015-9298-5

Dunbar RIM (1995) Neocortex size and group size in primates: a test of the hypothesis. J Hum Evol 28:287-296. https://doi.org/10.1006/jhev.1995.1021

Eisenberg JF (1981) The Mammalian Radiations. University of Chicago Press, Chicago

Ekdale EG (2010) Ontogenetic variation in the bony labyrinth of *Monodelphis domestica* (Mammalia: Marsupialia) following ossification of the inner ear cavities. Anat Rec 293:1896-1912

Elissamburu A (2012) Estimación de la masa corporal en géneros del Orden Notoungulata. Estud Geol (Madrid) 68:91-111. https://doi.org/10.3989/egeol.40336.133

Farris JS (1970) Methods for computing Wagner trees. Syst Zool 19:83-92. https://doi.org/10.2307/2412028

Felsenstein J (1985) Confidence limits on phylogenetics: an approach using bootstrap. Evolution 39:783-791. https://doi.org/10.1111/j.1558-5646.1985.tb00420.x

Fernández-Monescillo M, Antoine P-O, Pujos F, Gomes Rodrigues H, Mamani Quispe M, Orliac M (2019) Virtual endocast morphology of Mesotheriidae (Mammalia, Notoungulata, Typotheria): new insights and implications on notoungulate encephalization and brain evolution. J Mammal Evol 26:85–100. https://doi.org/10.1007/s10914-017-9416-7

Ferreira JD, Negri FR, Sánchez-Villagra MR, Kerber L (2020) Small within the largest: brain size and anatomy of the extinct *Neoepiblema acreensis*, a giant rodent from the Neotropics. Biol Lett 16:20190914. https://doi.org/10.1098/rsbl.2019.0914

Flynn JJ, Croft DA, Charrier R, Wyss AR, Hérail G, García M (2005) New Mesotheriidae (Mammalia, Notoungulata, Typotheria), geochronology and tectonics of the Caragua area, northernmost Chile. J S Am Earth Sci 19:55-74. https://doi.org/10.1016/j.jsames.2004.06.007

Gabbert SL (1997) The auditory and posterior cranial anatomy of the Toxodontia (Order Notoungulata) and its implications for higher level relationships. Dissertation, Columbia University, New York

García-López DA, Babot MJ (2015) Notoungulate faunas of northwestern Argentina: new findings of early-diverging forms from the Eocene Geste Formation. J Syst Palaeontol 13:557-579. https://doi.org/10.1080/14772019.2014.930527

García-López DA, Babot MJ (2017) Adiciones al conocimiento de los Campanorcidae (Notounglata, Typotheria) en el noroeste argentino. XX Congreso Geológico Argentino, San Miguel de Tucumán

Geisler JH, Uhen MD (2003) Morphological support for a close relationship between hippos and whales. J Vertebr Paleontol 23:991-996. https://doi.org/10.1671/32

Goloboff PA (1993) Estimating character weights during tree search. Cladistics 9:83-91. https://doi.org/10.1006/clad.1993.1003

Goloboff PA (1999) Analyzing large data sets in reasonable times: solutions for composite optima. Cladistics 15:415-428. https://doi.org/10.1111/j.1096-0031.1999.tb00278.x

Goloboff PA, Farris JS (2001) Methods for quick consensus estimate. Cladistics 17:S26-S34. https://doi.org/10.1111/j.1096-0031.2001.tb00102.x

Goloboff PA, Carpenter JM, Arias JS, Miranda Esqivel DR (2008a) Weighting against homoplasy improves phylogenetic analysis of morphological data sets. Cladistics 24:1-16. https://doi.org/10.1111/j.1096-0031.2008.00209.x

Goloboff PA, Farris JS, Nixon KC (2008b) T.N.T., a free program for phylogenetic analysis. Cladistics 24:774-786. https://doi.org/10.1111/j.1096-0031.2008.00217.x

Goloboff PA, Torres A, Arias JS (2018a) Weighted parsimony outperforms other methods of phylogenetic inference under models appropriate for morphology. Cladistics 34:407-437. https://doi.org/10.1111/cla.12205

Goloboff PA, Torres A, Arias JS (2018b) Parsimony and model-based phylogenetic methods for morphological data: comments on O'Reilly, et al. Palaeontology 61:625-630. https://doi.org/10.1111/pala.12353

Gray H (1977) Anatomy, Descriptive and Surgical, 15th ed. Crown Publishers, New York

Hitz RB, Flynn JJ, Wyss AR (2006) New basal Interatheriidae (Typotheria, Notoungulata, Mammalia) from the Paleogene of central Chile. Am Mus Novitates 3520:1-32. https://doi.org/10.1206/0003-0082(2006)3520/1:NBITNM/2.0.CO;2

Hitz RB, Reguero M, Wyss AR, Flynn JJ (2000) New interatheriines (Interatheriidae, Notoungulata) from the Paleogene of central Chile and southern Argentina. Fieldiana Geol (New Series) 42:1-26. https://doi.org/10.5962/bhl.title.5169

Horovitz I (2000) The tarsus of *Ukhaatherium nessovi* (Eutheria, Mammalia) from the Late Cretaceous of Mongolia: an appraisal of the evolution of the ankle in basal therians. J Vertebr Paleontol 20:547-560. https://doi.org/10.1671/0272-4634(2000)020/0547:TTOUNE/2.0.CO;2

Horovitz I (2004) Eutherian mammal systematics and the origins of South American ungulates as based on postcranial osteology. Bull Carnegie Mus Nat Hist 36:63-79. https://doi.org/10.2992/0145-9058(2004)36/63:EMSATO/2.0.CO;2

Jerison HJ (1973) Evolution of the Brain and Intelligence. Academic Press, New York

Kay RF, Vizcaíno SF, Bargo MS (2012) A review of the paleoenvironment and paleoecology of the Miocene Santa Cruz Formation. In: Vizcaíno SF, Kay RF, Bargo MS (eds) Early Miocene Paleobiology in Patagonia: High-Latitude Paleocommunities of the Santa Cruz Formation. Cambridge University Press, Cambridge, pp 331–365. https://doi.org/10.1017/CBO9780511667381.018

Kielan-Jaworowska Z (1983) Multituberculate endocranial casts. Palaeovertebrata 13:1-12

Kielan-Jaworowska Z (1984) Evolution of the therian mammals in the late Cretaceous of Asia. Part VI. Endocranial casts of eutherian mammals. Palaeontol Pol 46:157-171

Kielan-Jaworowska Z (1986) Brain evolution in Mesozoic mammals. In: Flanagan KM, Lillegraven JA (eds) Vertebrates, Phylogeny, and Philosophy. Contrib Geol Spec Pap 3, Univ Wyoming, pp 21–34

Kielan-Jaworowska Z (1997) Characters of multituberculates neglected in phylogenetic analyses of early mammals. Lethaia 29:249-266. https://doi.org/10.1111/j.1502-3931.1996.tb01658.x

Kramarz AG, Bond M (2014) Critical revision of the alleged delayed dental eruption in South American "ungulates." Mammal Biol 79:170-175. https://doi.org/10.1016/j.mambio.2013.11.001

Krombach GA, Schmitz-Rode T, Prescher A, DiMartino E, Weidner J, Günther RW (2002) The petromastoid canal on computed tomography. Eur Radiol 12:2770-2775. https://doi.org/10.1007/s00330-002-1306-5

López-Torres S, Bertrand OC, Lang MM, Silcox MT, Fostowicz-Frelik Ł (2020) Cranial endocast of the stem lagomorph *Megalagus* and brain structure of basal Euarchontoglires. Proc R Soc B 287:20200665. https://doi.org/10.1098/rspb.2020.0665

Macrini TE (2006) The evolution of endocranial space in mammals and non-mammalian cynodonts. Dissertation, University of Texas at Austin

Macrini TE (2009) Description of a digital cranial endocast of *Bathygenys reevesi* (Merycoidodontidae; Oreodonta) and implications for apomorphy-based diagnosis of isolated, natural endocasts. J Vertebr Paleontol 29:1199-1211

Macrini TE, Flynn JJ, Croft DA, Wyss AR (2010) Inner ear of a notoungulate placental mammal: anatomical description and examination of potentially phylogenetically informative characters. J Anat 216:600-610. https://doi.org/10.1111/j.1469-7580.2010.01224.x

Macrini TE, Flynn JJ, Ni X, Croft DA, Wyss AR (2013) Comparative study of notoungulate (Placentalia, Mammalia) bony labyrinths and new phylogenetically informative inner ear characters. J Anat 223:442-461. https://doi.org/10.1111/joa.12108

Macrini TE, Muizon C, de Cifelli RL, Rowe T (2007a) Digital cranial endocast of *Pucadelphys andinus*, a Paleocene metatherian. J Vertebr Paleontol 27:99-107. https://doi.org/10.1671/0272-4634(2007)27/99:DCEOPA/2.0.CO;2

Macrini TE, Rougier GW, Rowe T (2007b) Description of a cranial endocast from the fossil mammal *Vincelestes neuquenianus* (Theriiformes) and its relevance to the evolution of endocranial characters in therians. Anat Rec 290:875-892. https://doi.org/10.1002/ar.20551

Macrini TE, Rowe T, VandeBerg JL (2007c) Cranial endocasts from a growth series of *Monodelphis domestica* (Didelphidae,

Marsupialia): a study of individual and ontogenetic variation. J Morphol 268:844-865. https://doi.org/10.1002/jmor.10556
Macrini TE, Rowe T, Archer M (2006) Description of a cranial endocast from a fossil platypus, *Obdurodon dicksoni* (Monotremata, Ornithorhynchidae), and the relevance of endocranial characters to monotreme monophyly. J Morphol 267:1000-1015. https://doi.org/10.1002/jmor.10452
Madden RH (1997) A new toxodontid notoungulate. In: Kay RF, Madden RH, Cifelli RL, Flynn JJ (eds) Vertebrate Paleontology in the Neotropics: the Miocene Fauna of La Venta, Colombia. Smithsonian Institution Press, Washington, DC, pp 335-354
Maddison WP (1991) Squared-change parsimony reconstructions of ancestral states for continuous-valued characters on a phylogenetic tree. Syst Biol 40: 304-314. https://doi.org/10.1093/sysbio/40.3.304
Maddison WP, Maddison DR (2019) Mesquite: a modular system for evolutionary analysis. Version 3.61 http://www.mesquiteproject.org
Marquet PA, Taper ML (1998) On size and area: patterns of mammalian body size extremes across landmasses. Evol Ecol 12:127-139. https://doi.org/10.1023/A:1006567227154
Martínez G, Dozo MT, Vera B, Cerdeño E (2019) Paleoneurology, auditory region, and associated soft tissue inference in the late Oligocene notoungulates *Mendozahippus fierensis* and *Gualta cuyana* (Toxodontia) from central-western Argentina. J Vertebr Paleontol 39:6. https://doi.org/10.1080/02724634.2019.1725531
Meng J, Hu YM, Li CK (2003) The osteology of *Rhombomylus* (Mammalia, Glires): implications for phylogeny and evolution of Glires. Bull Am Mus Nat Hist 275:1-247
Muizon C de, Billet G, Argot C, Ladevèze S, Goussard F (2015) *Alcidedorbignya inopinata*, a basal pantodont (Placentalia, Mammalia) from the early Palaeocene of Bolivia: anatomy, phylogeny and palaeobiology. Geodiversitas 37:397-634. https://doi.org/10.5252/g2015n4a1
Nasif NL, Musalem S, Cerdeño E (2000) A new toxodont from the late Miocene of Catamarca, Argentina, and a phylogenetic analysis of the Toxodontidae. J Vertebr Paleontol 20:591-600. https://doi.org/10.1671/0272-4634(2000)020/0591:ANTFTL/2.0.CO;2
Ni X, Flynn JJ, Wyss AR, Zhang C (2019) Cranial endocast of a stem platyrrhine primate and ancestral brain conditions in anthropoids. Sci Adv 5:eaav7913. https://doi.org/10.1126/sciadv.aav7913
Nixon KC (1999) The parsimony ratchet, a new method for rapid parsimony analysis. Cladistics 15:407-414. https://doi.org/10.1111/j.1096-0031.1999.tb00277.x
O'Leary MA, Bloch JI, Flynn JJ, Gaudin TJ, Giallombardo A, Giannini NP, Goldberg SL, Kraatz BP, Luo Z-X, Meng J, Ni X, Novacek MJ, Perini FA, Randall ZS, Rougier GW, Sargis EJ, Silcox MT, Simmons NB, Spaulding M, Velazco PM, Weksler M, Wible JR, Cirranello AL (2013) The Placental Mammal Ancestor and the Post–K-Pg Radiation of Placentals. Science 339:662-667. https://doi.org/10.1126/science.1229237
Orliac MJ, Argot C, Gilissen E (2012) Digital cranial endocast of *Hyopsodus* (Mammalia, "Condylarthra"): a case of Paleogene terrestrial echolocation? PLoS One 7:e30000. https://doi.org/10.1371/journal.pone.0030000
Orliac MJ, O'Leary MA (2016) The inner ear of *Protungulatum* (Pan-Euungulata, Mammalia). J Mammal Evol 23:337-352. https://doi.org/10.1007/s10914-016-9327-z
Pascual R, Vucetich MG, Fernández J (1978) Los primeros mamíferos (Notoungulata, Henricosborniidae) de la Formación Mealla (Group Salta, Subgrupo Santa Barbara). Sus implicancias filogenéticas, taxonómicas y cronológicas. Ameghiniana 15:366-390
Patterson B (1934) *Trachytherus*, a typotherid from the Deseado Beds of Patagonia. Geol Ser Field Mus Nat Hist 6:119-139. https://doi.org/10.5962/bhl.title.5226
Patterson B (1937) Some notoungulate braincasts. Geol Ser Field Mus Nat Hist 6:273-301. https://doi.org/10.5962/bhl.title.5197
Patterson B (1977) A primitive pyrothere (Mammalia, Notoungulata) from the early Tertiary of northwestern Venezuela. Fieldiana Geol 33:397-422. https://doi.org/10.5962/bhl.title.5225
Patterson B, Pascual R (1968) The fossil mammal fauna of South America. Q Rev Biol 43:409-451
Radinsky L (1977) Brains of early carnivores. Paleobiology 3:333-349. https://doi.org/10.1017/S0094837300005509
Radinsky L (1978) Evolution of brain size in carnivores and ungulates. Am Nat 112:815-831
Radinsky L (1981) Brain evolution in extinct South American ungulates. Brain Behav Evol 18:169-187. https://doi.org/10.1159/000121785
Ravel A, Orliac MJ (2014) The inner ear morphology of the 'condylarthran' *Hyopsodus lepidus*. Hist Biol 27:957-969. https://doi.org/10.1080/08912963.2014.915823
Reguero MA, Prevosti FJ (2010) Rodent-like notoungulates (Typotheria) from Gran Barranca, Chubut Province, Argentina: phylogeny and systematics. In: Madden RH, Carlini AA, Vucetich MG, Kay RF (eds) The Paleontology of Gran Barranca: Evolution and Environmental Change through the Middle Cenozoic of Patagonia. Cambridge University Press, Cambridge, pp 152-169
Reguero MA, Ubilla M, Perea D (2003) A new species of *Eopachyrucos* (Mammalia, Notoungulata, Interatheriidae) from the late Oligocene of Uruguay. J Vertebr Paleontol 23:445-457. https://doi.org/10.1671/0272-4634(2003)023/0445:ANSOEM/2.0.CO;2
Riggs ES, Patterson B (1935) Description of some notoungulates from the Casamayor (*Notostylops*) beds of Patagonia. Proc Am Philos Soc 75:163-215.
Rodríguez-Gómez G, Cassini GH, Palmqvist P, Bargo MS, Toledo N, Martín-González JA, Muñoz NA, Kay RF, Vizcaíno SF (2020) Testing the hypothesis of an impoverished predator guild in the early Miocene ecosystems of Patagonia: an analysis of meat availability and competition intensity among carnivores. Palaeogeogr Palaeoclimatol Palaeoecol 554:109805. https://doi.org/10.1016/j.palaeo.2020.109805
Rose KD (2006) The Beginning of the Age of Mammals. Johns Hopkins University Press, Baltimore
Rowe T, Macrini TE, Luo Z-X (2011) Fossil evidence on origin of the mammalian brain. Science 332:955-957. https://doi.org/10.1126/science.1203117
Sánchez-Villagra MR (2002) The cerebellar paraflocculus and the subarcuate fossa in *Monodelphis domestica* and other marsupial mammals - ontogeny and phylogeny of a brain-skull interaction. Acta Theriol 47:1-14. https://doi.org/10.1007/BF03193561
Scarano AC, Carlini AA, Illius AW (2011) Interatheriidae (Typotheria; Notoungulata), body size and paleoecology characterization. Mammal Biol 76:109-114. https://doi.org/10.1016/j.mambio.2010.08.001
Shockey BJ (1997) Two new notoungulates (Family Notohippidae) from the Salla Beds of Bolivia (Deseadan: late Oligocene): systematics and functional morphology. J Vertebr Paleontol 17:584-599. https://doi.org/10.1080/02724634.1997.10011005
Shockey BJ, Flynn JJ (2007) Morphological diversity in the postcranial skeleton of Casamayoran (?Middle to Late Eocene) Notoungulata and foot posture in notoungulates. Am Mus Novitates 3601:1-26.
Shockey BJ, Flynn JJ, Croft DA, Gans P, Wyss AR (2012) New leontiniid Notoungulata (Mammalia) from Chile and Argentina: comparative anatomy, character analysis, and phylogenetic hypotheses. Am Mus Novitates 3737:1-64
Shultz S, Dunbar R (2010) Encephalization is not a universal macroevolutionary phenomenon in mammals but is associated with sociality. Proc Nat Acad Sci 107:21582-21586. https://doi.org/10.1073/pnas.1005246107

Simpson GG (1932) Skulls and brains of some mammals from the *Notostylops* beds of Patagonia. Am Mus Novitates 578:1-11

Simpson GG (1933a) Braincasts of *Phenacodus*, *Notostylops*, and *Rhyphodon*. Am Mus Novitates 622:1-19

Simpson GG (1933b) Braincasts of two typotheres and a litoptern. Am Mus Novitates 629:1-18

Simpson GG (1948) The beginning of the age of mammals in South America. Bull Am Mus Nat Hist 91:1-232

Simpson GG (1980) Splendid Isolation: The Curious History of South American Mammals. Yale University Press, New Haven

Stankowich T, Romero AN (2017) The correlated evolution of antipredator defences and brain size in mammals. Proc R Soc B 284:20161857. https://doi.org/10.1098/rspb.2016.1857

Stirton RA (1953) A new genus of interatheres from the Miocene of Columbia. Univ Calif Publ Geol Sci 29:265-348

Striedter GF (2005) Principles of Brain Evolution. Sinauer Associates, Sunderland

Symonds MRE, Blomberg SP (2014) A primer on phylogenetic generalised least squares. In: Garamszegi LZ (ed) Modern Phylogenetic Comparative Methods and Their Application in Evolutionary Biology. Springer, Heidelberg, pp 105-130

van der Geer A, Lyras D, de Vos J, Dermitzakis M (2010) Evolution of Island Mammals: Adaptation and Extinction of Placental Mammals on Islands. John Wiley & Sons, Chichester

Vera B (2012) Postcranial morphology of *Notopithecus* Ameghino, 1897 (Notoungulata, Interatheriidae) from the middle Eocene of Patagonia, Argentina. J Vertebr Paleontol 32:1135-1148. https://doi.org/10.1080/02724634.2012.694320

Vera B (2016) Phylogenetic revision of the South American notopithecines (Mammalia, Notoungulata). J Syst Palaeontol 14:461-480.

Welker F, Collins MJ, Thomas JA, Wadsley M, Brace S, Cappellini E, Turvey ST, Reguero M, Gelfo JN, Kramarz A, Burger J, Thomas-Oates J, Ashford DA, Ashton PD, Rowsell K, Porter DM, Kessler B, Fischer R, Baessmann C, Kaspar S, Olsen JV, Kiley P, Elliott JA, Kelstrup CD, Mullin V, Hofreiter M, Willerslev E, Hublin J-J, Orlando L, Barnes I, MacPhee RDE (2015) Ancient proteins resolve the evolutionary history of Darwin's South American ungulates. Nature 522:81-84. https://doi.org/10.1038/nature14249

Westbury M, Baleka S, Barlow A, Hartmann S, Paijmans JLA, Kramarz A, Forasiepi AM, Bond, M, Gelfo JN, Reguero MA, López-Mendoza P, Taglioretti M, Scaglia F, Rinderknecht A, Jones W, Mena F, Billet G, Muizon C de, Aguilar JL, MacPhee RDE, Hofreiter M (2017) A mitogenomic timetree for Darwin's enigmatic South American mammal *Macrauchenia patachonica*. Nat Commun 8:15951. https://doi.org/10.1038/ncomms15951

Wyss AR, Flynn JJ, Croft DA (2018) New Paleogene notohippids and leontiniids (Toxodontia; Notoungulata; Mammalia) from the early Oligocene Tinguiririca fauna of the Andean main range, central Chile. Am Mus Novitates 3903:1-42. https://doi.org/10.1206/3903.1